Front page

Exam information
NFYK10020E - Physics Thesis 60 ECTS, Niels Bohr Institute - Contract:136274 (Anirudh Bhatnagar)

Handed in by
Anirudh Bhatnagar
zsv531@alumni.ku.dk

Exam administrators
Eksamensteam, tel 35 33 64 57
eksamen@science.ku.dk

Assessors
Mauricio Bustamante
Examiner
Mbustamante@nbi.ku.dk
+4535334778

Steen Lynge Hannestad
Co-examiner
steen@phys.au.dk

Hand-in information

Title: Probing Quantum Gravity Decoherence in High-Energy Neutrinos from the Active Galaxy NGC1068
Title, english: Probing Quantum Gravity Decoherence in High-Energy Neutrinos from the Active Galaxy NGC1068
The sworn statement: Yes
Does the hand-in contain confidential material: No

UNIVERSITY OF COPENHAGEN

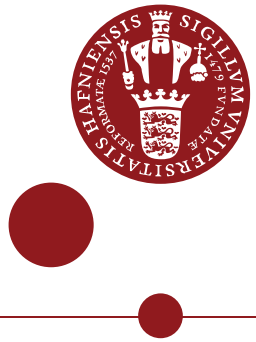

Masters Thesis

Probing Quantum-Gravity Decoherence in High-Energy Neutrinos from the Active Galaxy NGC 1068

Anirudh Bhatnagar

Supervised by Mauricio Bustamente

November 2023

Anirudh Bhatnagar

Probing Quantum-Gravity Decoherence in High-Energy Neutrinos from the Active Galaxy NGC 1068

Masters Thesis, November 2023
Supervisors: **Mauricio Bustamente**

University of Copenhagen
Niels Bohr International Academy
Blegdamsvej 17
2100 Copenhagen N

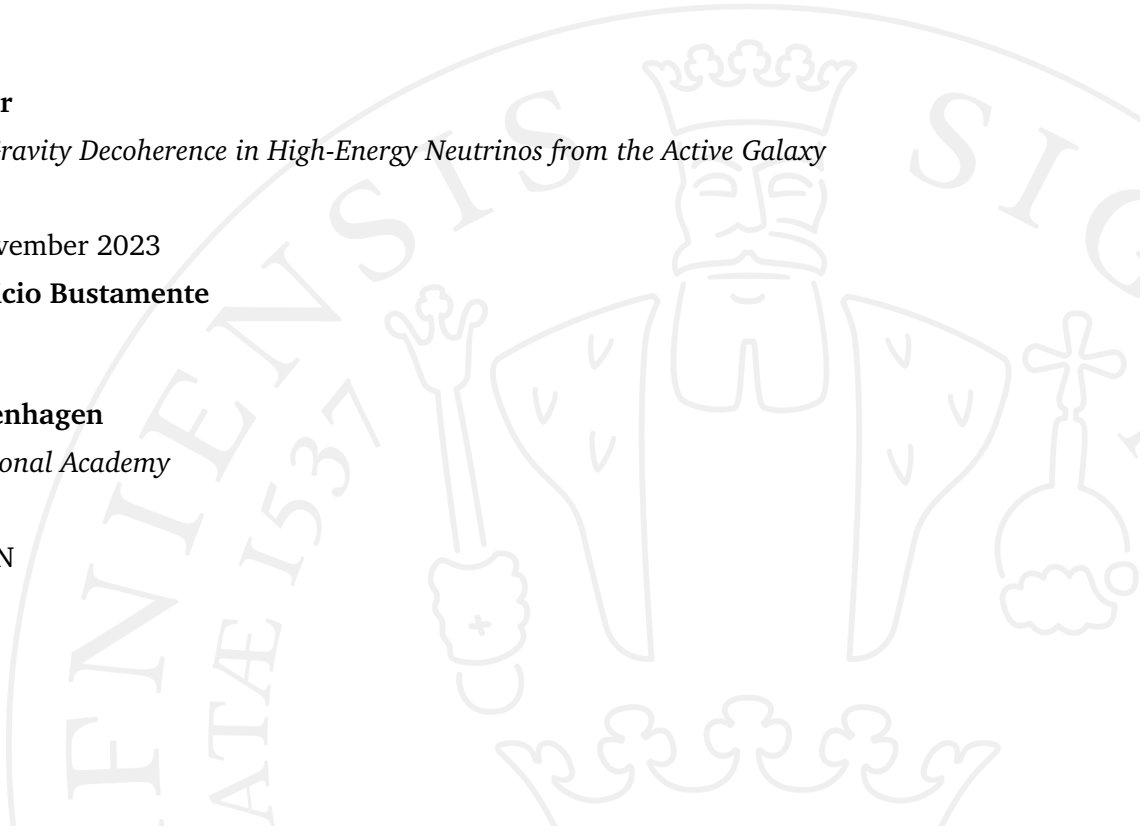

Acknowledgements

I would like to thank my supervisor, Mauricio Bustamente for all his guidance and patience with me. I really appreciated all the times you took aside and helped me through any areas of confusion. Thank you for going above and beyond at certain times to accommodate me. I would also like to thank my group members of He-Nu (Bernanda, Victor and Damiano), for assisting me along the thesis and improving my understanding on this subject. I have a better grasp of the subject matter in this field simply due to interactions within this group.

I also want to give a special thank you to all my friends in Copenhagen for just being there. I appreciate all of you. I would also like to thank the Masters office group (OGB) to stick by this program and never let it feel like a dull day.

Finally, a big thank you to my family for supporting me through any hurdles I have or may face. I appreciate every one of you from the bottom of my heart.

I could not have finished this thesis without the support of this mixture of wonderful people and I am looking forward for the next chapter.

Abstract

The recent discovery of high-energy neutrinos from an active galactic nuclei; NGC1068, by the IceCube detector marked a significant breakthrough in the field. This discovery has not only opened up an array of new opportunities to probe high-energy neutrino physics but also confirm the first steady-state source of such neutrinos. We exploit the advantages of a stable, continuous source, in contrast to the diffuse flux of neutrinos commonly employed in most experiments. This allows us to discern subtle deviations from standard physics within the energy spectrum of the high-energy neutrinos. In this thesis, we focus on the subtleties introduced by quantum gravity effects in the form of quantum decoherence in the three neutrino framework. These effects are observed through exploring a promising case of neutrino interaction with virtual black holes created in the extreme case of Planck scale fluctuations in space-time. We aim to differentiate between standard and decohered oscillations by effectively bounding the decoherence phase space. We are able to exclude standard oscillations in the decoherence phase space up to a 1σ confidence limit, allowing the excluded region to be investigated for measurable effects of quantum gravity in high-energy neutrinos.

Contents

1 Introduction **1**

2 Overview of Neutrino Theory **3**

2.1 Standard Neutrino Oscillations 4

2.1.1 Standard oscillations in vacuum 4

2.1.2 Standard Oscillations In Matter 11

2.2 Astrophysical Neutrinos 15

2.2.1 NGC1068 18

2.3 Quantum Decoherence in Astrophysical Neutrinos 20

3 Methodology **28**

3.1 IceCube Neutrino Observatory 29

3.2 Quantum Decoherence vs Standard Oscillations 31

3.2.1 Calculation of Event Rates In IceCube 35

3.3 Statistical Analysis 38

3.3.1 Absence of Atmospheric background flux 41

4 Results **44**

5 Summary and Outlook **48**

6 Appendix A **50**

6.0.1 Physical Constants 50

6.0.2 Density Matrix Formalism 50

6.0.3 Dependent Parameters of Functions 52

7 Bibliography **53**

1 Introduction

The exploration of the universe is approached through a diverse array of multi-messenger signals; electromagnetic radiation, gravitational waves, cosmic rays, and neutrinos, each offering a unique view. Due to the weak interactive nature of neutrinos with matter, they tend to be an excellent tool in the epoch of multi-messenger astronomy used to study our universe and bring us insight into stellar objects which might be opaque to other multi-messengers. This unique property allows neutrinos to bring unimpeded information about their sources and play a vital role in studying stellar interiors. The detection of these cosmic high-energy neutrinos from astrophysical sources has progressively improved over the past few decades due to heightened focus in advancements in neutrino detectors.

One of the groundbreaking detection of cosmic neutrinos came from the supernova named SN1987A [30]. It was unique as it was observed in almost all wavelengths of the multi-messengers and confirmed the first evidence of neutrino emission from a core-collapse supernova with energies of about 10 MeV. These neutrino events were detected in multiple neutrino detectors starting at Kamiokande II followed by IMB and Baksan. Between May 2010 and May 2012, IceCube claims to have detected 28 high-energy neutrinos above the energy range of 30 TeV from unknown astrophysical sources, ushering into the realm of high-energy neutrino detection [29]. Prior to this discovery, we strictly had evidence of low energy neutrino emission by two sources: SN1987A and the sun [28,29]. The progression continued and in 2017 IceCube detected a 290 TeV muon neutrino event from the blazar: TXS 0506 + 056, finding the first candidate of a high-energy neutrino source [31]. In 2022, the IceCube collaboration confirmed the first detection of high-energy neutrinos from the active galactic nuclei NGC1068, becoming the first steady-state source of high-energy neutrinos detected by this telescope [16]. Directional analysis of all neutrino events recorded at this detector confirmed that the neutrino events ($\sim$ 80 at TeV energy scale) detected by NGC1068 contributed to the most excess number of high-energy neutrinos recorded by any neutrino source [24].

This AGN is measured to be at a distance of 14 Mpc [16], offering us the opportunity to test high-energy neutrino physics over long propagation distances of neutrinos to Earth, including new physics. Utilizing a steady-state neutrino source, we exclude the uncertainties present in tests used in neutrino physics that depend on a diffuse flux of neutrinos. This diffuse flux of neutrinos corresponds to unknown number of neutrino sources located at unknown distances, emitting neutrinos of an unknown energy distribution. Thus by removing these uncertainties, we can look for minuscule features in the energy spectrum of neutrinos that could indicate non-standard neutrino physics.

We focus on features induced by quantum-gravity effects on a propagating neutrino emitted by the NGC1068 en-route to Earth. We examine the effects of quantum gravity on the propagating neutrinos by studying the scenario of neutrino interaction with virtual black holes, produced by fluctuations in space-time. These fluctuations are assumed to be created at Planck scales and any evidence of quantum decoherence in a neutrino system can also open up a window for experimentation into Planck scale physics.

This thesis is divided into four sections starting from developing the theory of neutrino propagation in vacuum and matter. Building on this foundation, we delve into astrophysical neutrinos and introduce NGC1068. The theoretical section is concluded by establishing quantum decoherence effects in astrophysical neutrinos. In the following section, we develop the methods used to detect these quantum decoherence effects in open quantum systems, which is usually favored for investigating neutrino decoherence. The detection principle of IceCube is reviewed and we recognize the challenges in distinguishing standard oscillations from decoherence induced by quantum gravity in detected neutrino events. In the final two sections we discuss the distinctive limits in the decoherence phase space we could establish isolating standard oscillations from decohered neutrinos and discuss the possibility of future work in this subject matter.

2

Overview of Neutrino Theory

Neutrinos are classified under the Standard Model as neutral counterparts of leptons. There are three generations or flavors of neutrinos: electron (ν_e), muon (ν_μ), and tau (ν_τ) , corresponding to the three leptons in the Standard Model. Neutrinos solely interact weakly in nature through charged current(CC) and neutral current(NC) interactions which are mediated by the W and Z bosons respectively [7]. This will be further delved into in subsequent sections of this chapter. Neutrinos have been under the microscope for a brief amount of time now and due to their unique properties, play a vital role in our understanding of the Universe.

In this chapter, I will review:

- Standard Neutrino Oscillations
- Astrophysical Neutrinos
- Quantum decoherence in astrophysical neutrinos

2.1 Standard Neutrino Oscillations

2.1.1 Standard oscillations in vacuum

In the Standard Model of particle physics, neutrinos are considered massless particles. However, several experiments have proved that neutrinos undergo a change in flavor as it propagates over a varying distance. This phenomenon was first observed in atmospheric neutrinos at the Super-Kamikande experiment [32]. The experiment decisively showed the existence of a flavor change by reporting a deficit number of atmospheric muon neutrinos compared to the expected counts calculated considering no oscillations. These oscillations between flavor neutrinos proved the existence of a non-zero mass of these neutrinos, viewed as a superposition of mass eigenstates defining the flavor neutrino state. This relation can be observed in the definition of the flavor state [7]:

$$|\nu_\alpha\rangle = \sum_k U^*_{\alpha k}|\nu_k\rangle, \tag{2.1}$$

where $U^*_{\alpha k}$ represents the associated amplitude of a particular mass eigenstate which is given by the elements of the Pontecorvo–Maki–Nakagawa–Sakata (PMNS) matrix described in equation(2.3) and $\alpha = e$,μ, τ, and $|\nu_k\rangle$ are the mass eigenstates with $k = 1, 2, 3$.
The massive neutrino states(ν_k) in equation (2.1) obeys the Schrödinger equation,

$$H|\nu_k\rangle = E_k|\nu_k\rangle, \tag{2.2}$$

with energy eigenvalues $E_k = \sqrt{p^2 + m_k^2}$, thereby evolving the mass eigenstates as plane waves. The composition of the mass eigenstates of a flavor neutrino is governed by the constants of nature as dictated in the PMNS matrix. The PMNS matrix can be divided into three matrices providing a framework describing the mixing between neutrino flavor states along with their corresponding mass eigenstates [7]:

$$U_{3x3} = \begin{bmatrix} 1 & 0 & 0 \\ 0 & c_{23} & s_{23} \\ 0 & -s_{23} & c_{23} \end{bmatrix} \begin{bmatrix} c_{13} & 0 & s_{13}e^{-i\delta_{CP}} \\ 0 & 1 & 0 \\ -s_{13}e^{i\delta_{CP}} & 0 & c_{13} \end{bmatrix} \begin{bmatrix} c_{12} & s_{12} & 0 \\ -s_{12} & c_{12} & 0 \\ 0 & 0 & 1 \end{bmatrix}, \quad (2.3)$$

from left to right the matrices describe the Atmospheric, Reactor and Solar. The c_{ij} and s_{ij} are the sine and cosine of the mixing angles (ij): θ_{12}, θ_{13}, θ_{23}, between the active neutrinos and δ_{CP} is the CP violation phase. CP violation has been scrutinized by two prominent neutrino oscillation experiments evaluating this phase in the leptonic sector, namely the T2k in Japan [42] and NoVa in the USA [41].

The product of the above three matrices results in a 3x3 unitary PMNS matrix governing the oscillations between the ν_e, ν_μ and ν_τ neutrinos. The unitarity of U forces the mass states and in retrospect, the flavor states to be orthonormal in nature [7].

$$\langle \nu_j | \nu_k \rangle = \delta_{jk}; \quad (2.4)$$

$$\langle \nu_\alpha | \nu_\beta \rangle = \delta_{\alpha\beta} \quad (2.5)$$

Each flavor state is thus described by the periodically propagating mass eigenstates traversing at different velocities, giving rise to transitions or oscillations between one flavor to another. The evolution of the flavor state to see the transition between the two states $|\nu_\beta>$ is made evident by implementing equation(2.1-2.2):

$$\begin{aligned} |\nu_\alpha(t)\rangle &= \sum_{\beta=e,\mu,\tau} \sum_k U^*_{\alpha k} \exp(-iE_k t) U_{\beta k} |\nu_\beta\rangle \\ &= \sum_{\beta=e,\mu,\tau} \sum_k U^*_{\alpha k} \exp(-iHt) U_{\beta k} |\nu_\beta\rangle, \end{aligned} \quad (2.6)$$

which is defined as the probability amplitude of the transitions i.e $< \nu_\beta | \nu_\alpha >$. These oscillations are observed as an interference phenomenon among the neutrino mass eigenstates if the neutrinos are considered massive and the mass and flavor states do not align with each other. Due to the relativistic nature of neutrinos we can assume $\mathrm{L} \sim \mathrm{t}$ and $\mathrm{E} \approx |p|$. With these assumptions we can simplify the energy eigenvalues (E_k) by realizing the mass of the neutrino is significantly smaller than its momentum $m_k \ll |p|$ and thus approximating the energy eigenvalues in equation(2.2) as $E_k = |p| + \frac{m_k^2}{2|p|}$ which leads to the final formulation of the phase factor as $E_k \approx E + \frac{m_k^2}{2E}$. We can disregard

any contributions from exp(-iEL) as it acts as a global phase on all the mass eigenstates. Using these approximations, we can calculate the probability of the transitions between two flavor neutrino states by using equation(2.6).

$$\begin{aligned} |<\nu_\beta|\nu_\alpha>|^2 = P_{\alpha\beta} = P_{\nu_\alpha\to\nu_\beta}(L) &= |\sum_{k,j} U^*_{\alpha k}U_{\beta k}|^2 \exp(-i(E_k - E_j)t) \\ &= \sum_{k>j} U^*_{\alpha k}U_{\beta k}U_{\alpha j}U^*_{\beta k} \exp\left(\frac{-i\Delta m^2_{kj}L}{2E}\right) \end{aligned} \tag{2.7}$$

This equation describes a periodic oscillation probability between two flavours in vacuum. The information of the oscillatory behavior is contained in the phase factor with $\Delta m^2_{kj} = m^2_k - m^2_j$ describing the mass difference between two massive neutrinos. This probability also emphasizes the existence of a non-zero mass of a neutrino. Cosmologists have been able to successfully set an upper bound on the sum of the three mass states ($\sum_{i=1}^{3} m_{\nu_i} \leq 0.12$ eV)[43]. The smallest difference between the mass states $\sim 7.41 \cdot 10^{-5}$eV^2 was discovered in Δm^2_{21}, describing the mass difference of the solar neutrinos. Since the difference is positive, we can conclude that $m_2 > m_1$. However, the uncertainty arises in considering the mass difference $m_{3i} \sim \pm 2.5 \cdot 10^{-3}$eV^2. The sign raises doubts on whether $\Delta m^2_{31} > \Delta m^2_{32}$ or vice versa, pointing out the uncertainty in the absolute value of the mass eigenstate (m_3 & m_2). This has led to two hierarchies of mass difference: normal ordering and inverted ordering. In the normal ordering we assume the masses ($m_3 > m_2$) and inverted ordering has the proportionality reversed ($m_2 > m_3$). In this thesis, we assume a normal ordered hierarchy of the massive neutrinos. The oscillation probability is directly proportional to the propagation distance of neutrinos and we can infer an inversely proportional dependence of energy with the propagation distance ($\sim \frac{1}{2E}$) .

There are two rules emerging from this equation due to the unitarity of the PMNS matrix [7].

1. The sum of the probabilities from a flavor neutrino (ν_α) to all flavor neutrinos(ν_β) ($\nu_\alpha = \nu_\beta$) equals 1 and thus the same argument will hold for the probability of transitioned flavor neutrino (ν_β) from a flavor neutrino (ν_α).

$$\sum_\alpha = P_{\alpha\beta} = \sum_\beta = P_{\alpha\beta} = 1$$

We can explicitly define the oscillation probability for a three neutrino system given in equation (2.7) by expanding the phase factor and using the unitarity condition set up by the mixing matrix(U):

$$P_{\alpha\beta}(L,E) = \Delta_{\alpha\beta} - 4\sum_{k>j}\mathrm{Re}[U^*_{\alpha k}U_{\beta k}U_{\alpha j}U^*_{\beta k}]\sin^2\left(\frac{\Delta m^2_{kj}L}{4E}\right) \pm 2\sum_{k>j}\mathrm{Im}[U^*_{\alpha k}U_{\beta k}U_{\alpha j}U^*_{\beta k}]\sin\left(\frac{\Delta m^2_{kj}L}{2E}\right), \tag{2.8}$$

leading to the neutrino and antineutrino transition probability in a three neutrino framework, with the negative sign in the imaginary part representing the antineutrino probability. The oscillation probability depends on the elements of the mixing matrix (U). The transition probability is dictated by equation (2.8) with $\alpha \neq \beta$ while the survival probability is calculated with $\alpha = \beta$. The $\Delta = 1$ for the survival probability ($\alpha = \alpha$) and $\Delta = 0$ for the transitions due to the orthonormal assumptions in equations (2.4-2.5). The quartic products from the PMNS matrix does not depend on the specific parametrization of the PMNS matrix or even the oscillatory phase factor. These quartic products are infact invariant under rephasing transformation i.e. $U_{\alpha k} \rightarrow \exp(i\ \phi_k)U_{\alpha k}\exp(i\ \psi_\alpha)$. The CP and T violations in neutrino oscillations are defined by the mixing terms in the PMNS matrix. In a three neutrino framework, the mixing matrix is complex and contains a CP violation factor to accommodate for this behavior in the reactor part of the matrix. To measure these CP violations, experiments must be sensitive to the oscillatory behaviour of the neutrino and antineutrino transition probabilities [41-42]. If we subtract the probabilities of neutrino and antineutrino equations, the resultant would yield an expression sensitive to CP violations in neutrino systems. This is evident by examining the surviving imaginary part of the probability in equation(2.9).

$$A^{CP}_{\alpha\beta} = P_{\nu_\alpha\rightarrow\nu_\beta}(L,E) - P_{\bar{\nu}_\alpha\rightarrow\bar{\nu}_\beta}(L,E)$$

$$A^{CP}_{\alpha\beta} = 4\sum_{k>j}\mathrm{Im}[U^*_{\alpha k}U_{\beta k}U_{\alpha j}U^*_{\beta k}]\sin\left(\frac{\Delta m^2_{kj}L}{2E}\right) \tag{2.9}$$

For practical purposes, we can approximate the three neutrino framework to a two neutrino mixing scenario as experiments are not sensitive towards the influence of the three neutrino mixing, and can only accommodate mixing information between two neutrinos. The benefits of working in this framework is a smaller number of uncertain parameters and a simplified PMNS

matrix. This framework is however not used in the main analysis of the this thesis and is just included as a simplified model to explain neutrino oscillations.

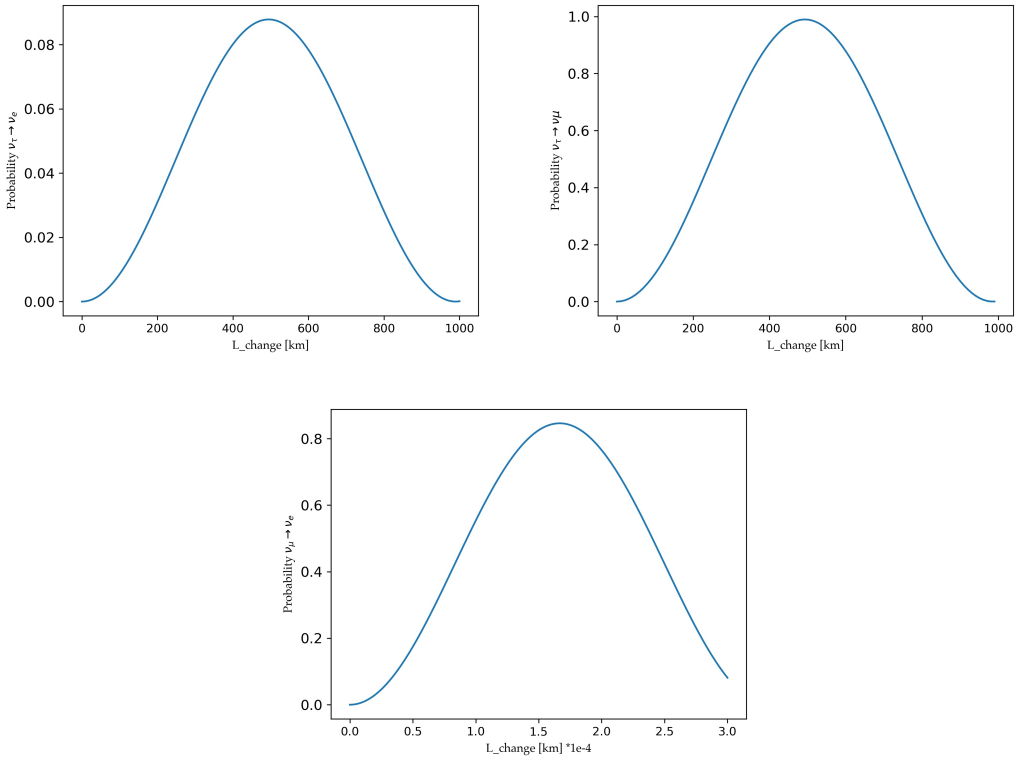

Figure 2.1: The transitional probability of a two neutrino system in vaccuum considering 1 GeV neutrinos. The two mass differences used for calculating the transitional probabilities ; $\Delta m^2_{21} \approx 7.41 \cdot 10^{-5}\ eV^2$ for the bottom graph and the top two graphs were constructed with $\Delta m^2_{31} \approx 2.5 \cdot 10^{-3}$eV^2 and $\Delta m^2_{32} \approx 2.43 \cdot 10^{-3}$eV^2. The mixing angles used in the PMNS matrix in these graphs were extracted from [18].

The neutrino flavor states are in a simplified linear superposition of the mass states. The flavor state could be pure flavor states $(\nu_\alpha = \nu_e, \nu_\mu)$ or a linear combination of pure flavor states $(\nu_\beta = c1\nu_\mu + c2\nu_\tau)$, with $c1^2 + c2^2 = 1$. The transition or the survival probability is now dictated by a simplified 2x2 unitary PMNS matrix [7]:

$$U_{2x2} = \begin{bmatrix} \cos\theta & \sin\theta \\ -\sin\theta & \cos\theta \end{bmatrix}, \tag{2.10}$$

in which $0 < \theta < \pi/2$ and the $\Delta m^2_{kj} \rightarrow \Delta m^2_{21}$, thereby ignoring the contributions from the third massive neutrino. Considering a two neutrino system $(|\nu_e\rangle|\nu_\mu\rangle)$, the transitions would be dictated by the the mixing of the two mass eigenstates ν_1 and ν_2 represented in the Hamiltonian in the mass basis by a

2x2 diagoanlized matrix: diag $\left(\frac{m_1^2}{2E}, \frac{m_2^2}{2E}\right)$. Thus we can simplify the components of the PMNS matrix in equation (2.8) by substituting the elements of the 2x2 PMNS matrix for the $(|\nu_e\rangle \rightarrow |\nu_\mu\rangle)$ transitions

$$P_{\nu_e \rightarrow \nu_\mu} = [U_{e2}^* U_{\mu 2} U_{e1} U_{\mu 1}^*],$$

leaving us with the fully developed transitional probability of a two neutrino system in natural units ($\hbar = c = 1$)

$$P_{\nu_\alpha \rightarrow \nu_\beta}(L, E) = \sin^2 2\theta \sin^2 \left(\frac{\Delta m^2 L}{4E}\right) \tag{2.11}$$

,
with the recovery of survival probability embedded in the equation; $P_{\alpha\alpha}$ = 1-$P_{\alpha\beta}$. Additionally, if we include the factors of '$\hbar$' and 'c', we can reframe the transitional probability from an experimental standpoint.

$$P_{\nu_\alpha \rightarrow \nu_\beta}(L, E) = \sin^2 2\theta \sin^2 \left(\frac{1.27 \Delta m^2 (eV^2) L(km)}{E(GeV)}\right)$$

The L/E dependence seen in the above equation is used to describe the oscillation length (L^{osc}) of the transition probability between two flavor states. Oscillation length describes the distance it takes for of a complete oscillation from one flavor neutrino to another, which is evident in figure (2.1). Thus we can constraint the value of the oscillation length $\sim$ propagation distance (L) since the oscillations won't occur for $L < L^{osc}$ and for $L > L^{osc}$, the oscillations would be averaged or incoherent over the propagated distance. So considering these constraints, we can describe the oscillation length ($L^{osc} = \frac{4E}{\Delta m^2} \sim 1$).One important revelation from the transition probability is the degeneracy caused in the $\sin^2 2\theta$ due to the limits on the angle (θ). Angles below and above a certain value of theta will favor a massive neutrino over an other describing a flavor neutrino. This will be mended in the next section when we tackle standard oscillations in matter.

Another conventional way to calculate the probabilities of flavor transitions is by using the Hamiltonian in the flavor basis. This representation of the Hamiltonian in the flavor basis can be used to directly evaluate the evolved flavor state (α) at a given time.

$$|\nu_\alpha(L)\rangle = \exp(-iH_f L)|\nu_\alpha\rangle$$

From equation(2.1), we can switch back and forth from mass basis to flavor basis by a simple trick: $H_f = UH_mU^+$, with H_m describing the mass basis in vacuum for the $(|\nu_e\rangle \rightarrow |\nu_\mu\rangle)$ transitions written in a more convenient way

$$H_m = \begin{bmatrix} \frac{m_1^2}{2E} & 0 \\ 0 & -\frac{m_2^2}{2E} \end{bmatrix} \rightarrow \begin{bmatrix} \frac{\Delta m^2}{4E} & 0 \\ 0 & -\frac{\Delta m^2}{4E} \end{bmatrix},$$

by subtracting $\frac{m_1^2}{2E}$ and a global phase of $\frac{\Delta m^2}{4E}$ from the mass Hamiltonian. Thus we can define the Hamiltonian in the flavor basis as follows:

$$H_f = \begin{bmatrix} \cos\theta & \sin\theta \\ -\sin\theta & \cos\theta \end{bmatrix} \begin{bmatrix} \frac{\Delta m^2 L}{4E} & 0 \\ 0 & -\frac{\Delta m^2 L}{4E} \end{bmatrix} \begin{bmatrix} \cos\theta & -\sin\theta \\ \sin\theta & \cos\theta \end{bmatrix} \tag{2.12}$$

$$= \left(\frac{\Delta m^2 L}{4E}\right) \begin{bmatrix} -\cos 2\theta & \sin 2\theta \\ \sin 2\theta & \cos 2\theta \end{bmatrix}$$

This representation still obeys the Schrodinger's equation and evolves the flavor states as plane waves. However, to calculate the oscillation probability, we need to reverse the equated Hamiltonians, since its still represented in the flavor basis i.e. $H_m = U^+ H_f U$ considering its a widely accepted notion that neutrinos propagate in the mass basis. This representation of the Hamiltonian will be seen in the next section when we explore the effects of matter on neutrino oscillations.

2.1.2 Standard Oscillations In Matter

In this section, we will investigate the effects of a matter profile on neutrino oscillations. In the previous section we explored the freely propagating neutrinos in vacuum exposed to no external stimulus. However, neutrinos propagating in matter are now privy to external factors like varying density profiles in the medium which will affect their oscillation probabilities. Neutrinos propagating in matter undergo coherent forward elastic scattering and almost negligible incoherent scatterings with other particles in a medium. These interactions can be charged current(CC) or neutral current(NC) via the exchange of a W and a Z boson respectively. These scattering processes leads to generating charged current(V_{CC}) responsible for inelastic scattering processes and neutral current(V_{NC}) potentials leading to elastic scattering.

We will develop the Hamiltonian for neutrino oscillations in matter assuming a two-neutrino system. The Hamiltonian describing the oscillation probability is now a sum of the vacuum Hamiltonian developed in equation(2.12) with an additional matter term including the contributions from CC and NC interactions [7]:

$$H_M = H_{vac} + V_W \begin{bmatrix} 1 & 0 \\ 0 & 0 \end{bmatrix} + V_Z \begin{bmatrix} 1 & 0 \\ 0 & 1 \end{bmatrix} \tag{2.13}$$

H_M represents the Hamiltonian of neutrino oscillations in matter as a sum of vacuum and matter interactions. However, NC interactions governed by Z boson will affect all flavors equally by introducing a global phase in the oscillation amplitude, and only contributions from CC interactions with an electron are taken into consideration, signified by the top left corner of the CC interaction matrix. So this is the only interaction allowed by the W mediator amongst the three neutrino flavors.

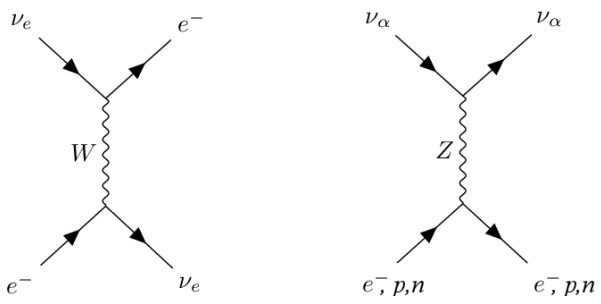

Figure 2.2: CC and NC interaction of neutrino with matter. [7]

By calculating the Feynmann diagrams in figure (2.2), we can calculate the effective potentials for both these processes. The CC potential in matter works out to $\sqrt{2}G_f N_e$ while the NC potential is $\sqrt{2}G_f N_n$,if we consider a electrically neutral medium. This will force the coherent forward scattering off electrons and protons to cancel each other and have contributions solely from neutrons. The $[N_n, N_e$]are the number density of neutrons and electrons respectively per unit volume.

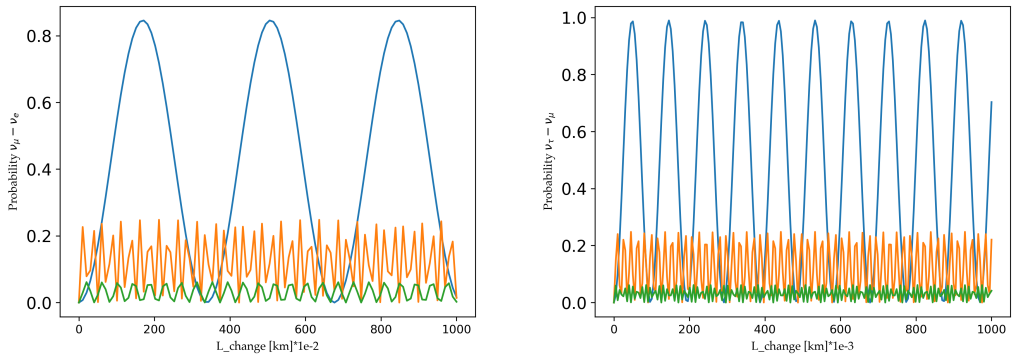

Figure 2.3: The transition probability of flavor neutrinos in varying density profiles of matter (Orange and green) compared to oscillations in vacuum (blue). The values of the mass differences and the mixing angles used in the PMNS matrix were extracted from [18]. The graphs depict the oscillation probability in the density profiles of magnitudes of $7.84 \cdot 10^{-19} cm^{-3}$ (orange) and $1.56 \cdot 10^{-18} cm^{-3}$(green).

The amplitude of the oscillations are severely damped in matter and are inversely proportional to the size of the density profile which we can notice in the graphs comparing vacuum amplitudes of the oscillation probability (blue) to the matter induced oscillations in density profiles in the vicinity of $10 \cdot 10^{-20} cm^{-3}$. Even slightly bigger density profiles can damp the oscillation amplitudes as seen in the top right graph. Oscillations are still roughly coherent for $\nu_\mu \rightarrow \nu_e$ transitions at a dense profile of 10^{-18} but we see almost a complete loss of coherence for ν_τ transitions within the first few kilometers of the propagated distance. The oscillations are extremely rapid in comparison to vacuum oscillations, mimicking the distinctive traits of astrophysical high-energy neutrinos that have propagated over cosmic distances which is astounding, considering that the simulations were performed on a 1000 km baseline.

We can write the Hamiltonian in a matrix representation of the flavor basis.The Hamiltonian in equation(2.13) can be rephrased as:

$$H_M = H_{vac} + \frac{V_W}{2}\begin{bmatrix} 1 & 0 \\ 0 & -1 \end{bmatrix}$$

$$= \frac{\Delta m^2}{4E}\begin{bmatrix} -(\cos 2\theta - A_{CC}) & \sin 2\theta \\ \sin 2\theta & \cos 2\theta - A_{CC} \end{bmatrix} \tag{2.14}$$

in which A_{CC} is the effective potential encountered in any specified matter profile given by $\frac{V_W^2/2}{\Delta m^2/4E} = \frac{2\sqrt{2}G_f N_e E}{\Delta m^2}$

Including the matter counterparts from equations(2.15-2.16) into equation(2.14), we regain the original shape of the vacuum Hamiltonian in the flavor basis written in terms of the matter Hamiltonian.

$$\Delta m_M = \Delta m^2 \sqrt{sin^2\theta + (cos2\theta - A_{cc})^2} \tag{2.15}$$

$$\sin^2 2\theta_M = \frac{\sin^2 2\theta}{\sin^2 2\theta + (\cos 2\theta - A_{cc})^2} \tag{2.16}$$

$$H_M = \frac{\Delta m_M^2}{4E}\begin{bmatrix} -\cos 2\theta_M & \sin 2\theta_M \\ \sin 2\theta_M & \cos 2\theta_M \end{bmatrix} \tag{2.17}$$

Therefore, A_{CC} measures the importance of matter effect compared to the squared neutrino mass difference. From the normalisation factors when A_{CC} equals $cos2\theta$ there is maximal/equal mixing of these mass states referred to as the Mikheyev-Smirnov-Wolfenstein(MSW) resonance. This resonance is apparent in the figure(2.4) where it is clearly observed at 45°, leading to the possibility of total transitions between two flavours.

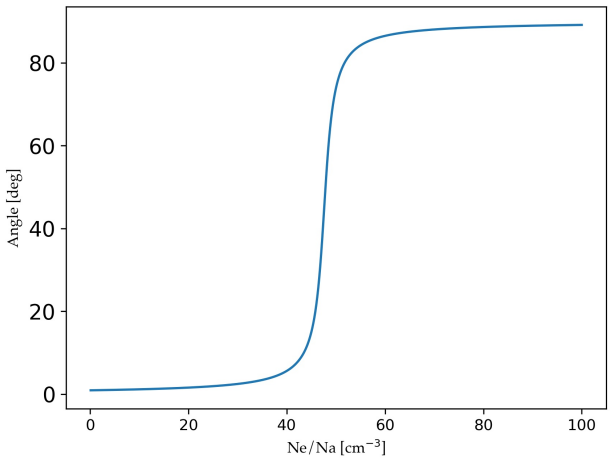

Figure 2.4: Effective mixing angle vs the Number density of electrons (N_e). This shows the MSW resonance for $m_{21} = 7.65 \cdot 10^{-5}$ eV^2 with the effective vacuum mixing angle of $sin^2\theta = 10^{-3}$ and E = 1 MeV. The resonance is clear at $\theta = 45°$.The Avagadro's number is given by N_a.

The figure(2.4) provides a unique conclusion between the number density of electrons in a medium and the mixing angle in matter between neutrino states. For certain values of N_e/N_a, we can see resonance between neutrino states regardless of the value of the vacuum angle. This can be seen more clearly by defining the mixing angle in matter,

$$\tan 2\theta_M = \frac{\tan 2\theta}{1 - \frac{A_{CC}}{\cos 2\theta}}$$

where resonance will occur at $A_{CC} = \cos 2\theta$. These particular values for the number density can be explicitly showcased by solving for the resonant number density of electrons in a given medium for a fixed neutrino energy used in equation(2.14):

$$N_e^R = \frac{\Delta m^2 \cos 2\theta}{2\sqrt{2} G_f E}$$

So, when the neutrino reaches these resonance (MSW) values i.e. at $\theta_M = \frac{\pi}{4}$, the neutrino system reverts to its vacuum expectation values as evident in equations (2.15-2.16).

The matter effects discussed in this section are however not observed in high-energy astrophysical neutrinos. We will be modifying the probability functions developed in the vacuum section which is used for the final analysis in this literature.

2.2 Astrophysical Neutrinos

High-energy neutrinos in the range of TeV-PeV detected on Earth come from astrophysical sources. They have emerged as one of the pivotal instruments to study the universe as they carry unhindered information about their origins due to their weakly interacting nature, with the drawback of difficult detection due to this property. However, with advancements in detector size and technology combined with an improved theoretical understanding of these particles, there has been a major improvement in confirmed counts of astrophysical neutrinos. Within this decade, IceCube has detected astrophysical neutrino fluxes of up to 10 PeV [24]. IceCube first reported the discovery of high-energy astrophysical neutrinos just three years after its completion in 2013, with 28 high-energy neutrinos [29]. After this breakthrough, IceCube has been able to detect 700,000 high-energy astrophysical and atmospheric neutrinos ranging from 100 GeV-1 PeV [24]. The high-energy spectrum of neutrinos detected at IceCube range from solar neutrinos ($E_\nu \approx 10^3 - 10^6$ eV)to high-energy neutrinos from cosmic rays($E_\nu > 10^{15} eV$) [24]. We will focus on the high-energy spectrum of neutrinos in the range of 1-10 TeV emitted by the active galactic nucleus(AGN) NGC1068 [16].

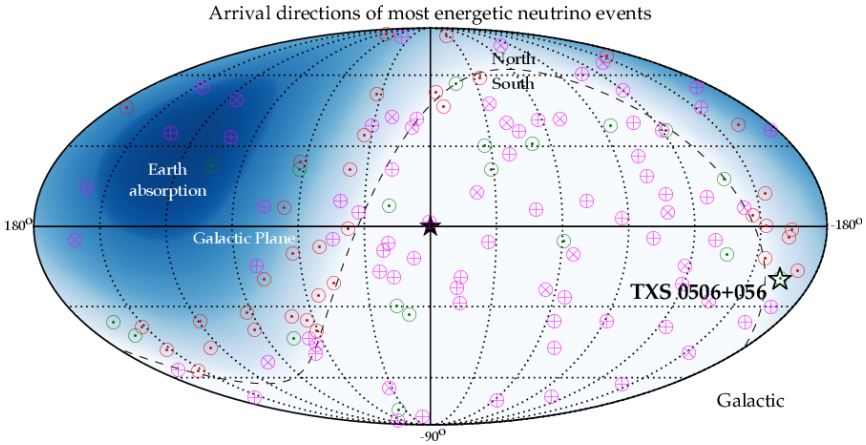

Figure 2.5: The figure above displays the arrival directions of high-energy neutrino events detected on Earth by IceCube. The red dot circles represents the upgoing track events, the high-energy starting events (HESE) (tracks $\otimes$ and cascades $\oplus$) and additional events in green. The blue region indicates the earth absorption of 100 TeV neutrinos and the dashed lines are equatorial plane. [27]

These high-energy neutrinos undergo rapid oscillations which shortens the oscillation length ($L_{osc} \sim \frac{1}{2E}$). The high energies of these neutrinos along with the distance makes it impossible to detect the oscillatory behavior of active flavor neutrinos discussed in the previous section of vacuum oscillations. To put into perspective, a 1 TeV neutrino propagating from an astrophysical source has an oscillation length of 0.1 pc,which is 8% of the way to Proxima Centauri. However, these neutrinos usually travel over hundreds of Mpc or Gpc. Thus, we measure the average oscillation probability of these incoming neutrinos. The transition or survival probability of standard oscillations shown in section(2.1.1) boils down to an incoherent probability [7].

$$\langle P_{\nu_\alpha \to \nu_\beta} \rangle = \sum_k |U_{\alpha k}|^2 |U_{\beta k}|^2. \tag{2.18}$$

One of the pressing open questions in high-energy astrophysics is to discover the sources of high-energy cosmic rays. There is evidence of high-energy cosmic particle accelerators from detection of high-energy cosmic particles like protons. However, these particles divert in direction due to magnetic fields while propagating to Earth. Cosmic neutrinos and photons are thus one of the better options to gain information about these cosmic accelerators as their travel path is unaffected by these magnetic fields [38]. These messengers are created whenever cosmic rays interact with light or ambient matter in the accelerator sites. The non-interactive nature of neutrinos was seen as an advantage to pursue information about extreme cosmic accelerators like active galactic nuclei(AGN) [34]. These AGN are powered by the accretion flow of matter into the supermassive black hole which is surrounded by a dusty torus obscuring the observable characteristics of the AGN. An AGN can project a narrow jet of plasma known as a blazar, which can be detected if its in the Earth's viewing angle [36]. The first source of a high-energy neutrino emission was recorded by a gamma-ray blazar TXS 0506+056. Other significant detections of neutrino events by IceCube have come from the direction of two blazars, PKS 1424+240 and GB6 J1542+6129; and now recently by the AGN, NGC1068 [37]. NGC1068 is however the first steady-state source of high-energy neutrino emission recorded by IceCube and the source we consider in this thesis. Due to certainty of the source distance to Earth, NGC1068 offers us the possibility to test high-energy neutrino physics during the propagation time of the neutrinos to the Earth, including looking for minute features in the energy spectrum of the neutrinos that may signal new neutrino physics.

Astrophysical sources studied by neutrino astronomy emit neutrinos in a ratio of three flavors ($\nu_e : \nu_\mu : \nu_\tau$). The sum of the ratio of the flavor neutrinos emitted by a source would always be unity ($\sum(\nu_e : \nu_\mu : \nu_\tau) = 1$). These flavor ratios are dictated by the processes responsible for their production and can change due to their environment [33]. Usually high-energy neutrinos are created through one of the two processes: inelastic proton-proton interactions (pp) or proton-photon interactions ($p\gamma$). Since AGN are known as sources of high energy γ rays, it's a valid assumption to presume $p\gamma$ interactions to be dominant [34]. These interactions produce delta baryons which eventually decay into pions and neutrons, finally decaying into neutrinos.

$$p + \gamma \rightarrow \Delta^+ \rightarrow \begin{pmatrix} n + \pi^+ \\ p + \pi^0 \end{pmatrix}$$

Parent Particle	Initial Decay	Final By-Products	Source Information
π^+	$\mu^+ + \nu_\mu$	$e^+ + \nu_e + \bar{\nu_\mu} + \nu_\mu$	Pion Beam
π^0	$\gamma + \gamma$	$\gamma + \gamma$	Cosmic Rays
n	$p + e^- + \nu_e$	$p + e^- + \nu_e$	Neutron Beam

Table 2.1: Decay Channel of delta baryon in a photohadronic process [35,16].

At low energies, neutron decays dominates the flux, splitting the number of events detected of each flavor in the ratio of ($N_{\nu_e} : N_{\nu_\mu} : N_{\nu_\tau}$=1 : 0 : 0). However at high energies the ratio is dictated by 1:2:0, due to the decay of charged pions. If the sources harbor intense magnetic fields, the intermediate muons cool via synchrotron radiation before decaying, so that the only high-energy neutrinos are ν_μ directly from the decay of pions. This yields the ratio of 0:1:0. The energy losses predominately affects the muons of the pion beam source($1 : 2 : 0$). The detected number of events has a flavor composition roughly around ($N_{\nu_e} : N_{\nu_\mu} : N_{\nu_\tau} \sim 1 : 1 : 1$) due to standard oscillations as seen in table(2.1). Later in this literature, we will find this unity ratio to be absolute when considering neutrino interactions with a virtual black hole over a certain magnitude and not just an approximation observed in standard oscillations. Since there is no measurement of the neutrino flavor composition in NGC1068, we focused our efforts on three ratio types:

Description	Flavor composition at source, f_s	Flavor ratio on earth, $f_\oplus$ (std)
Pion Beam Source	1: 2: 0	0.357: 0.325: 0.317
Neutron Beam Source	1: 0: 0	0.552: 0.260: 0.188
Muon Damped Source	0: 1: 0	0.260: 0.358: 0.382

Table 2.2: Ratio of flavor neutrinos ($\nu_e : \nu_\mu : \nu_\tau$) considered at the source of NGC1068 and the detected ratio of flavor neutrinos on earth via standard oscillations.

We will focus on neutrino propagation in standard oscillation and under the effect of quantum gravity in these three assumed source ratios of NGC1068 and try to distinguish between the detected ν_μ events from both these processes in the subsequent sections.

2.2.1 NGC1068

NGC1068 is a barred spiral galaxy which is part of the Cetus constellation. A barred spiral galaxy is a spiral galaxy with a central bar shaped structure composed of stars. It is often referred to as M77 discovered by Pierre Méchain in 1780 who had initially labelled it as a nebula [40]. The spectrum of M77 is peculiar and those features are seen in its broad emission lines indicating giant gas clouds rapidly moving out of the core of the galaxy at speeds of roughly 100 km/s; classifying NGC1068 as a Seyfert II galaxy [39,40].
A Seyfert galaxy is characterized as any class of spiral galaxy that has a compact bright nuclei characterized by variability of light intensity, emission of radio waves or spectra. These gas clouds are powered by an active galactic nucleus in the center of the galaxy [40]. The AGN is discovered to have a mass equal to 10 million solar masses through infrared observations by the California Institute of Technology. The core of M77 was discovered to be a good source of radio waves in 1952 by Berbard Yarnton Mills, and later confirmed when it was optically investigated by the Hubble space telescope. However, infrared investigation of the core by Caltech showed a strong support for characterization of a point-like source. The source has been studied for several years in X-ray, optical, UV, IR and radio wavelengths and recently in high-energy neutrinos.

IceCube detected 79^{+22}_{-20} ν_μ events from the direction of the NGC1068 over the course of 3186 days which allowed to pin the location of this active galaxy within a confidence region in the northern hemisphere [16]. The galaxy is

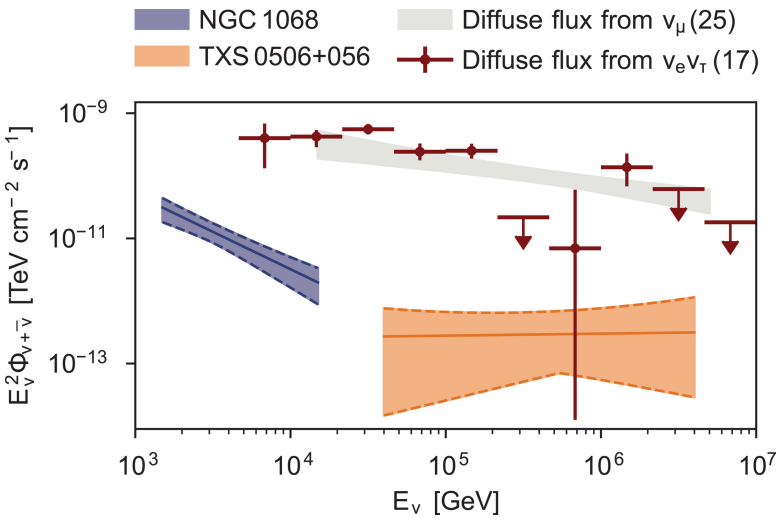

Figure 2.6: Flux comparison of point sources NGC1068 with TXS0506+056 at a 68% confidence region. The fluxes are given for a single flavor of neutrinos and antineutrinos assuming equal flavor ratio. Figure extracted from [16]

found to be at a distance of 14.4 Mpc in agreement with the literature which reported the AGN to be in a range from 10.3 ± 3 Mpc - 16.5 Mpc. The AGN was sighted at a declination of $(0^\circ)^{+0.3}_{-0.2}$, with a 95% confidence limit on the uncertainty. Neutrino emission from this galaxy ranged from 1 TeV-15 TeV, with most of them detected at 1 TeV. The detected flux was fitted on a generic power law spectrum:

$$\phi_{\nu_\mu+\bar{\nu}_\mu} = \phi_0 \frac{E_\nu}{E_0}^{-\gamma}, \tag{2.19}$$

with the flux normalized (E_0) at 1 TeV over a spectral index($\gamma = 3.2 \pm 0.2$) within 68% confidence region. The normalized flux (ϕ_0) recorded by IceCube was $(5 \pm 1.5_{stat} \pm 0.6_{sys}) \times 10^{-11}\ TeV^{-1}s^{-1}cm^{-2}$. If we assume similar ratio contributions from the other two flavors as observed through a pion decay beam in table(2.1), the total flux will be 3 times the detected muon neutrino flux. The systematic uncertainty in the flux arises from the deliberate variation of the flux normalization across different ice and detector properties to derive the best fit values of γ and ν_μ counts. If we assume an isotropic emission of the detected flux, the calculated redshift-corrected equivalent neutrino luminosity in the energy range of 1.5 TeV - 15 TeV at the fixed distance of 14.4 Mpc is (2.9± 1.1_{stat}) × 10^{42} erg s^{-1} which is 10 times brighter than the equivalent observed gamma ray luminosity (1.6 × 10^{41} erg s^{-1}) in the energy range of 100 MeV- 100 GeV [39].

The neutrino flux detected by the NGC1068 shows a strong evidence of future detection of high-energy neutrinos by an AGN. Figure(2.6) solidifies the presumption by comparing the flux detected by TXS0506+056 and AGN1068 to the total diffuse astrophysical flux. These two cosmic sources contribute 1% to the total diffuse flux in their respective energy ranges. Even though the energy range of NGC1068 does not match the diffuse flux, there is a possibility of contributions from other bright point sources or large populations of faint sources.

2.3 Quantum Decoherence in Astrophysical Neutrinos

Until now, we have analyzed neutrino oscillations in vacuum and matter. These particles are propagating in isolation from its environment as established in section(2.1). In this section we delve into the possibility of these astrophysical neutrinos coupling with its environment and observe the effects on the neutrino flavor composition detected on earth. In such a unique scenario, a neutrino would experience disturbance or complete destruction in coherence in their oscillations due to the Planck scale stochastic perturbations that will be introduced [9,26]. These perturbations should not be mistook for the Mikheyev-Smirnov-Wolfenstein(MSW) effect discussed in section(2.1.2) as that is a collective effect on all neutrinos propagating through that medium and thereby conserves coherence in neutrino oscillations.

We consider a possible candidate for the stochastic environment perturbing the propagating neutrino : a virtual black hole. If we assume gravity to be a quantum force, it can be hypothesized that space-time itself might be fluctuating at Planck scales,known as quantum foam or fuzzy space-time[9,10]. These fluctuations should influence the propagation of neutrinos over prolonged distances or time, referred to as lightcone fluctuations[10]. This deviated travel time would suggest an introduction of decoherence in the propagating neutrinos. In an extreme case, the magnitude of these fluctuations would be high enough that it would collapse to form virtual black holes of Planck lengths which would almost immediately evaporate at Planck time scales [10].

The magnitude of the effect of this decoherence on propagating neutrinos depends on how sensitive they are to Planck scale perturbations induced by these virtual black holes.

A neutrino encountering these virtual black holes should experience loss of quantum information or strong perturbations inflicted on their mass eigenstates. The impact of these perturbations are clearly observed in the damped average oscillation probability shown in [9] where the perturbations were added as a phase to a neutrino mass eigenstate leading to an incoherent average oscillation probability over prolonged distances. There are various indirect tests as outlined below, to gauge stochastic perturbations in neutrino oscillations, given the lack of an accepted model for quantum gravity [9]. We should be able to observe decoherence in the neutrino framework without adhering to the prolonged distance statute to measure lightcone fluctuations due to the extreme perturbation experienced by the neutrino [9-10].

The decoherence measured due to these perturbations need to be carefully accepted, as decoherence can be introduced in flavor states by other external factors. Some of these factors could include the resolution of the detector [44], or even effects from matter interactions of varied density profiles as observed in figure (2.3) portraying damped oscillatory behavior for flavor transitions. We can model the interactions of $(\nu - VBH)$ in the ways described below for a confirmation of quantum decoherence in the detected neutrinos. The level of quantum decoherence inflicted on these neutrino systems would directly be related to the particle's energy and its sensitivity to Planck sized fluctuations [8-10].

The four known possibilities we can venture for quantum decoherence effects [9]:

1. Mass state: The interaction collapses the superposition between the three mass eigenstates to a pure mass eigenstate with an equal probability of selecting either mass eigenstate.

2. Flavor state: The interaction collapses into a pure flavor state with an equal probability of selecting either flavor state.

3. Phase Perturbations: The neutrino experiences large random phase perturbations introduced in their mass states.

4. Neutrino Loss: The neutrino is lost in the interaction. This could be for various reasons. It could be absorbed by the virtual black hole or emitted in an opposite direction.

The mass state and flavor state scenarios rely on the same principle which would result in equal numbers of neutrinos from each flavor and mass states over long distances. Thus the average transitional probability of these neutrinos would adhere to $P(\nu_\alpha \rightarrow \nu_\beta) = \frac{1}{X}$, where X defines the number of families considered for the neutrino framework [9]. Over modest distances, flavor state scenarios can still accommodate for oscillations between different flavors with individual neutrinos out of phase from each other since the interaction occurs at random phases in their wavefunctions. However, the selection of a mass state obliterates the superposition effect of the three mass eigenstates which caused the oscillatory behavior of the time dependent evolution of flavor transitions. Flavor transitions are still permissible due to the mixing of flavor and mass states.
We focused on the second scenario where we assume the interaction to be elastic in nature and resulting in a pure flavor state. Due to the stochastic nature of these interactions, even though the neutrino might initially be in a well defined state, i.e a pure state, its true composition becomes increasingly difficult to predict as it propagates in time. A neutrino in such a random system can be treated as in an open quantum system [9]. This leads to considering the state of the neutrino as an ensemble of all possible quantum states with their associated probabilities. So the effects of decoherence forces a transition from a known quantum state to a mixed quantum state which can be defined through a density matrix [9].

$$\rho = \sum_j P_j |\psi_j\rangle\langle\psi_j|, \tag{2.20}$$

for j number of states with its associated probability, P_j, with the pure state described as $|\psi\rangle\langle\psi|$. The above density matrix evolves in time according to the Lindblad master equation [8],

$$\dot{\rho} = -i[H, \rho] - D[\rho]. \tag{2.21}$$

The first part of the equation(2.21) describes the standard behavior of the Hamiltonian i.e., standard oscillations while $D[\rho]$ is an operator describing the deviations from the norm,i.e., decoherence parameters. For a N-level neutrino system, where N describes the dimensionality of the system, we can generalize the evolving density matrix in SU(N) Hermitian basis by rewriting the Hamiltonian and the associated decoherence in its component form. The construction of the density matrix would be evident if we examine the component forms of each operator in the density matrix given in equation(2.21) [8].

$$\rho = \frac{1}{2}[\rho_o I + \rho_i \lambda_i],$$

$$H = \frac{1}{2}[h_o I + h_i \lambda_i],$$

$$D[\rho] = \frac{1}{2}[d_{\mu\nu}\rho_\nu \lambda_\mu],$$

where λ represents the generators of the SU(N) basis and I is the identity matrix. Thus we can rewrite the density matrix as [8],

$$\dot{\rho_\mu} = (h_{\mu\nu} + d_{\mu\nu})\rho_\nu \tag{2.22}$$

where $h_{\mu\nu}$ is usually fixed by the dimensions of the Hamiltonian. The $d_{\mu\nu}$ matrix can be simplified further by assuming the laws of thermodynamics still pertain to this situation, particularly the conservation of energy and an increase in entropy for spontaneous processes. For a non-zero decoherence operator, we can assume a linear increase in the entropy leading to hermiticity of operators and conservation of probability. If a quantum mechanical system is described by a density matrix, the entropy in consideration is defined as S(ρ) = -Tr($\rho ln \rho$), often referred to as the von-Neumann entropy [8,26]. In a finite-dimensional system, this entropy thus quantifies the transition from a pure quantum state to a mixed quantum state with the pure state describing a state with zero entropy(S(ρ) = 0). This would be helpful in building the density matrix with the pure state given by ρ_o showing standard oscillations as described in the 9x9 matrix[8,26]. The subscripts($\mu\nu$) are dictated by the flavors of the neutrino system. So, for a three level neutrino mixing, the density matrix is expressed in terms of the SU(3) basis vectors which are given by 8 Gell-Mann matrices (λ_i) and a 3x3 identity matrix. So the subscripts will range from $0 \leq \mu, \nu \leq 8$.

In summary, the evolution of the density matrix is described by 9×9 matrix with 11 decoherence parameters [8-10,26] which are represented as κ in this literature. The first row and column equal zero imposed by claiming $Tr(\rho) = 1$ and $Tr(\dot{\rho}) = 0$. The trace is thus preserved during evolution. The constraints set on the density matrix by the trace allowed us to conclude $\rho_0 = \frac{2}{3}$ as a constant in time [8-10]. The evolution of the density matrix with time is quantified by evaluating the effects of these decoherence parameters on the components of the initial density matrix(ρ_i):

$$\begin{bmatrix} \dot{\rho_o} \\ \dot{\rho_1} \\ \dot{\rho_2} \\ \dot{\rho_3} \\ \dot{\rho_4} \\ \dot{\rho_5} \\ \dot{\rho_6} \\ \dot{\rho_7} \\ \dot{\rho_8} \end{bmatrix} = \begin{bmatrix} 0 & 0 & 0 & 0 & 0 & 0 & 0 & 0 & 0 \\ 0 & A & B+\omega_{21} & 0 & 0 & 0 & 0 & 0 & 0 \\ 0 & B-\omega_{21} & \Lambda & 0 & 0 & 0 & 0 & 0 & 0 \\ 0 & 0 & 0 & \psi & 0 & 0 & 0 & 0 & 0 \\ 0 & 0 & 0 & 0 & x & y+\omega_{31} & 0 & 0 & 0 \\ 0 & 0 & 0 & 0 & y-\omega_{31} & z & 0 & 0 & 0 \\ 0 & 0 & 0 & 0 & 0 & 0 & a & b+\omega_{31} & 0 \\ 0 & 0 & 0 & 0 & 0 & 0 & b-\omega_{31} & \alpha & 0 \\ 0 & 0 & 0 & 0 & 0 & 0 & 0 & 0 & \delta \end{bmatrix} \begin{bmatrix} \rho_o \\ \rho_1 \\ \rho_2 \\ \rho_3 \\ \rho_4 \\ \rho_5 \\ \rho_6 \\ \rho_7 \\ \rho_8 \end{bmatrix},$$

where $\omega_{ij} = \Delta m^2_{jk}/4E$ and the non-zero terms describe decoherence parameters. The off- diagonal terms describe coherence between density states of the neutrino system. The coefficients B, y, b would have been essential if we had pursued the phase perturbation scenario of quantum decoherence. The diagonal describe the non-oscillatory terms which would correspond to the total density states.

The transition probability [8] of neutrinos is calculated by taking the trace of the product of the density matrices of a pure neutrino state ($t = 0$) with the neutrino state propagated over time,

$$P_{\alpha\beta} = \mathrm{Tr}[\rho_{\nu_\alpha(\mathrm{t})}\rho_{\nu_\beta(0)}],$$

where $\rho_{\nu_\alpha(t)}$ is the density matrix for a neutrino of a flavor ν_α at a certain time, $\rho_{\nu_\beta(0)}$ is the pure neutrino density matrix at $t = 0$ computed by 3×3 matrices [Appendix A] using the lindblad equation(2.21).

We can thereby solve for the transition probability of astrophysical neutrinos by using the above trace. Averaging over the phase factor($\exp(-i\frac{\Delta m^2_{kj} L}{4E})$) of the transitional probability developed in equation(2.8), makes the average flavor-transition probability sensitive to only two of the eleven mentioned de-

coherence parameters(ψ, δ) corresponding to the λ_3 and λ_8 of the decoherence matrix.

$$P_{\alpha\beta} = \frac{1}{3}+\frac{1}{2}(U^2_{\alpha1}-U^2_{\alpha2})(U^2_{\beta1}-U^2_{\beta2})D_\psi+\frac{1}{6}(U^2_{\alpha1}+U^2_{\alpha2}-2U^2_{\alpha3})(U^2_{\beta1}+U^2_{\beta2}-2U^2_{\beta3})D_\delta, \tag{2.23}$$

where $D_\psi = \exp(-2\psi t)$ and $D_\delta = \exp(-2\delta t)$ are the decoherence factors. These two decoherence coefficients damp the non-oscillatory density states of ρ_3 and ρ_8 leading the transitional probability to $\frac{1}{X}$. This expression is valid for astrophysical neutrinos, for which the probability has been averaged over cosmic distances. The damping factors can incorporate energy and distance dependence which will be explored in the methodology section. The lack of sensitivity of astrophysical neutrinos to the other decoherence parameters is due to the loss of coherence between density states [Appendix A], described through the damping of oscillations to zero by the off-diagonal decoherence coefficients. However, these decoherence parameters would be recovered for neutrinos travelling over modest distances like atmospheric neutrinos. The contribution of the damping factors can be explored further in these four cases [8]:

1) $\psi \neq 0$ and $\delta = 0$

$$P_{\alpha\beta} = \frac{1}{3} + \frac{1}{6}(U^2_{\alpha1} + U^2_{\alpha2} - 2U^2_{\alpha3})(U^2_{\beta1} + U^2_{\beta2} - 2U^2_{\beta3})$$

2) $\psi = 0$ and $\delta \neq 0$

$$P_{\alpha\beta} = \frac{1}{3} + \frac{1}{2}(U^2_{\alpha1} - U^2_{\alpha2})(U^2_{\beta1} - U^2_{\beta2})$$

3)$\psi = \delta = 0$

$$P_{\alpha\beta} = \sum_{i=1}^{3} |U_{\alpha i}|^2 |U_{\beta i}|^2$$

4)$\psi = \delta \neq 0$

$$P_{\alpha\beta} = \frac{1}{3}$$

When constraining decoherence, later, we focus on the latter, more general case, where decoherence renders all flavor-transition probabilities equal. We

will focus more in depth on the range of these damping constants in the later sections. The other options with the one of the damping constants equal to zero, the probability relies on the mixing matrix as seen with the recovery of the incoherent probability when both the parameters are zero. We will focus our efforts towards the third and fourth scenarios, comparing neutrinos in standard oscillations to neutrinos undergone quantum decoherence effects via the interaction with a virtual black hole.

These four probabilities are portrayed in the graphs shown below. We can notice the flavor ratios conforming to a single probability of exactly $\frac{1}{3}$ at roughly around 3 TeV which is referred to as a complete decoherence of the neutrino system in figure(2.7d). Our efforts would be focused in the transition region of neutrinos experiencing quantum decoherence with differentiable flavor composition to when the neutrino system is fully decohered. Flavor differentiation beyond the energies of 3 TeV neutrinos would be impossible to detect. The scenarios with even one of the decoherence parameters equal to zero is already shaping into the incoherent probability shown in figure (2.7b). The shifted values of the flavor ratios in figure (2.7a- 2.7b) shows the magnitude of decoherence a neutrino would experience even if one of the parameters is compatible to standard oscillations. However, the behavior of flavor ratios for $\delta = 0$ tends to be more compatible to standard oscillations than when assumed $\psi = 0$. This observation supports the idea of unequal contributions of decoherence inflicted on a neutrino by either parameter. In this particular case, δ appears to have a stronger contribution towards decoherence in neutrinos considering a bigger deviation from standard oscillations as observed figure (2.7b).

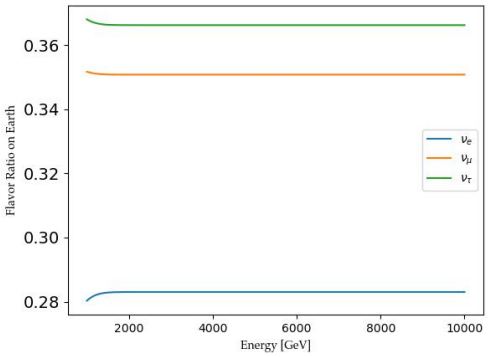

(a) $\delta = 0, \psi = 10^{-46}$ GeV^{-1}

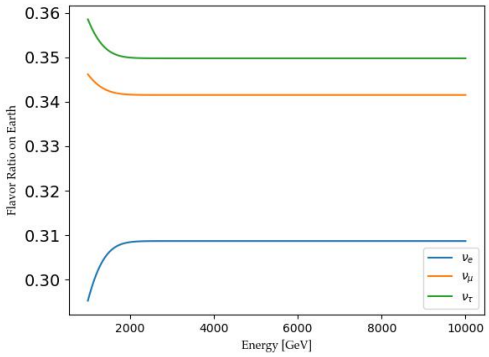

(b) $\psi = 0, \delta = 10^{-46}$ GeV^{-1}

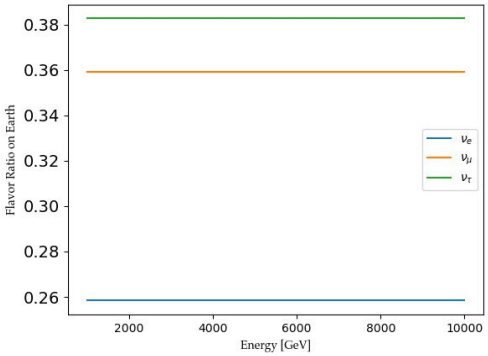

(c) $\psi = \delta = 0$

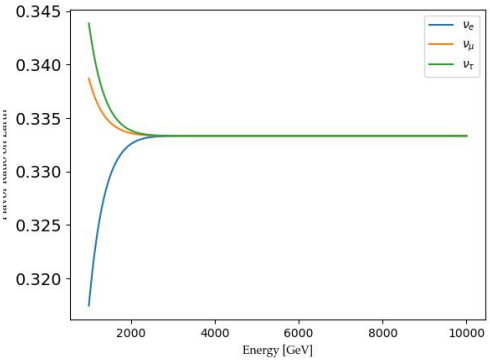

(d) $\psi = \delta = 10^{-46}$ GeV^{-1}

Figure 2.7: The graphs depict the flavor ratio of the three active neutrinos that will be detected on earth for the energy range of 1-10 TeV, portraying the four probabilities of astrophysical neutrinos experiencing quantum decoherence. These graphs were created assuming the source ratio of 0:1:0 of high-energy neutrino emission from NGC1068 with the incoming flux normalized at 1 TeV cm^{-2} s^{-1} sr^{-1}.

3 Methodology

After building a theoretical background in neutrino physics, the subsequent chapter will delve into the experimental setup to study these concepts in depth. We will focus our efforts towards differentiating the quantum decoherence effects in detected neutrino events from NGC1068, by the IceCube Neutrino Observatory.

In this chapter, I will review:

- IceCube Neutrino Observatory
- Standard oscillations vs quantum decoherence in neutrino events from NGC1068
- Statistical analysis

3.1 IceCube Neutrino Observatory

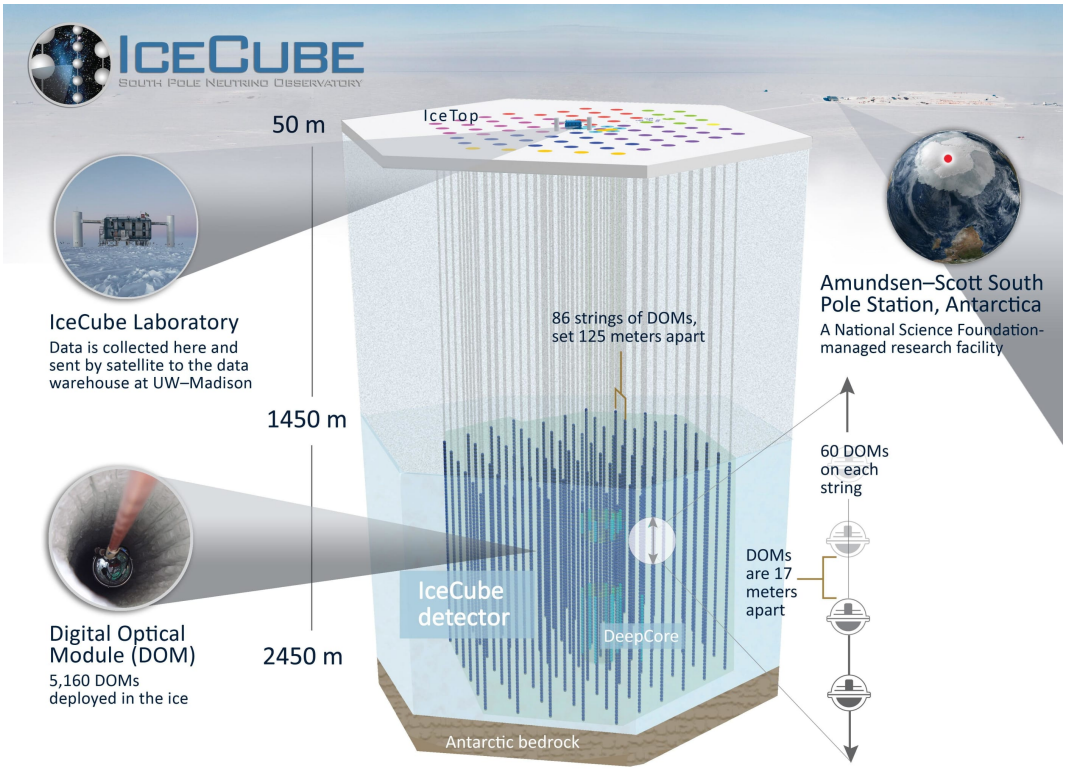

Figure 3.1: IceCube with its components and length measurements. [24]

The IceCube Neutrino observatory is the primary detector of this research. The constraints we manage to place in the decoherence phase space differentiating standard oscillations from decohered events are directly dependent on the observed neutrino events by this detector. IceCube has a volume of one cubic kilometer buried between 1.5 and 2.5 km underneath the surface of the Antarctic ice. There are 86 strings attached to this detector spaced at 125 meters from each other in a hexagonal grid. Each string has 60 digital optical modules containing a photomultiplier tube spaced at 17 meters apart. The spacing between eight of these strings are closer in the center at a horizontal distance of 70 meters with the digital optical modules at 7 meters apart [24].

In the ice, high-energy neutrinos(≥ 20 GeV) interact with matter via a charged-current(CC) or a neutral-current(NC) deep inelastic scattering, where the neutrino interacts with one of the constituent partons of neutrons or protons. A charged current interaction with a nucleon produces a corresponding lepton while a neutral current interaction produces a corresponding neutrino. Both these processes break up the nucleon. Charged final-state particles initiate high-energy particle showers that develop in the ice.

These final charged secondary particles emit Cherenkov radiation which is the result of particles travelling faster than the speed of light in a dielectric medium. This radiation is captured by the photomultiplier tubes(PMT) which converts these photons into an electric signal which is sent to the digital optical modules (DOM) [17,24].

Each flavor neutrino has its own signature which is read by the DOMs. Analysis of the light patterns and the amount of energy measured by the DOM's allows to estimate the energy and flavor of the incoming neutrino with a directional indicator for a specific neutrino flavor. The Cherenkov light is detected in three patterns: muon tracks created by CC interaction of ν_μ events, single and double cascades created by ν_e and ν_τ events respectively. A CC interaction of an ν_e and ν_τ with the nucleons in the ice creates these cascades which is the result of the two flavor neutrinos depositing most of their energy in a small region which are usually spherically spread across the DOM's. In the NC interactions, the hadronic showers are solely responsible for the cascades whereas in CC interactions these cascades are a sum of hadronic showers along with the inelastically scattered corresponding neutrino. There is a way to differentiate between the cascades of ν_e and ν_τ. A ν_τ event can leave a double cascade produced by the hadronic showers along with the second cascade occurring due to the decay of τ, thereby creating this double-bang signature. This process is somewhat rare and thus makes it hard for distinguishing between these two flavors. Another single cascade event detected at IceCube happens due to the interaction of anti-electron neutrino with an electron creating a W^- boson referred to as the Glashow resonance. Although these two flavors are excellent indicators to measure the energy distribution of the incoming neutrinos, they cannot be favored for directional information due to their large angular uncertainty [17,24].

The CC interaction of ν_μ with a nucleon in ice can provide us with directional information about the source as it leaves a trail along the strings known as tracks which are easily distinguishable in the detector. Currently, with an angular resolution of 1°, IceCube can confidently locate sources responsible for the emission of high-energy ν_μ with minimum statistical errors [25]. However, its a poor indicator for energy reconstruction as the muons exist the detector before depositing all its energy [24].

We will be relying on the muon tracks detected from the CC interactions of ν_μ, emitted by the point source: NGC1068.

3.2 Quantum Decoherence vs Standard Oscillations

We will depend on the average probability equation outlined in the theoretical section (2.3) incorporating the non-standard behavior of neutrino propagation described in equation (2.23). When the decoherence parameters are set to zero, we recover standard oscillations and conversely considering a non-zero decoherence parameter will induce quantum decoherence effects to the transitional probability function. This change in probability is evident in the number of muon events detected at IceCube.

We are familiar with the four ways to allocate for quantum decoherence effects in transitional probabilities. In this thesis, we will focus our attention towards detecting these effects in the propagating mass eigenstates. In such a case, we are assuming equal chance of either mass state to be selected by the $\nu - VBH$ elastic interaction. In this situation, NGC1068 is emitting flavor neutrinos propagating as a superposition of three mass eigenstates with their corresponding weights given by the PMNS matrix [7].

The interaction with a VBH collapses the planar wavefunctions into pure mass eigenstates [8-10]. Each mass eigenstate has an equal probability to be chosen, which is evident in the transitional probability distributions in figure (3.2), during complete decoherence situations when $P_{\alpha\beta} = \frac{1}{3}$. Intuitively,

not all magnitudes of a virtual black hole should be able to inflict complete decoherence within the mass eigenstate framework of a neutrino flavor. This is clearly observed in the varied flavor ratio of ν_e and ν_μ detected on earth for different decoherence values in figure(3.2). Since the neutrino detectors are not sensitive to oscillation effects in astrophysical high-energy neutrinos, we can consider these mass eigenstates propagating to earth adhering to the same conditions. On earth, these mass eigenstates are detected as flavor neutrinos with our focus directed towards the ν_μ events.

Quantum decoherence effects in neutrino systems is an elusive property measuring the loss of coherence in the quantum state of neutrinos arising from neutrino interactions with its surrounding environment. The ratio of $(\nu_e : \nu_\mu : \nu_\tau)$ events detected in standard oscillations from an astrophysical source does not exactly pertain to equal proportions of the three flavors on Earth as shown in table(2.1). However, when these neutrinos undergo an interaction with a virtual black hole above a certain magnitude, this ratio becomes definitively equal; i.e, $(\nu_e : \nu_\mu : \nu_\tau) \equiv (1 : 1 : 1)$ [8-10]. The proof of quantum decoherence effects in neutrino systems poses its own challenges such as the limited information available from the detected astrophysical neutrinos along with the complexity of the cosmic environment. Considering the limited number of ν_μ events comprising the data sample [16], detection of quantum decoherence effects in the number of events detected at IceCube already starts off as a daunting task.

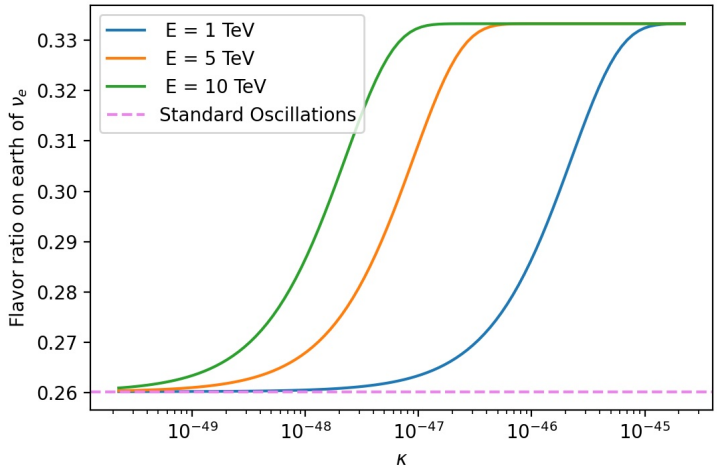

(a) Electron flavor content at Earth

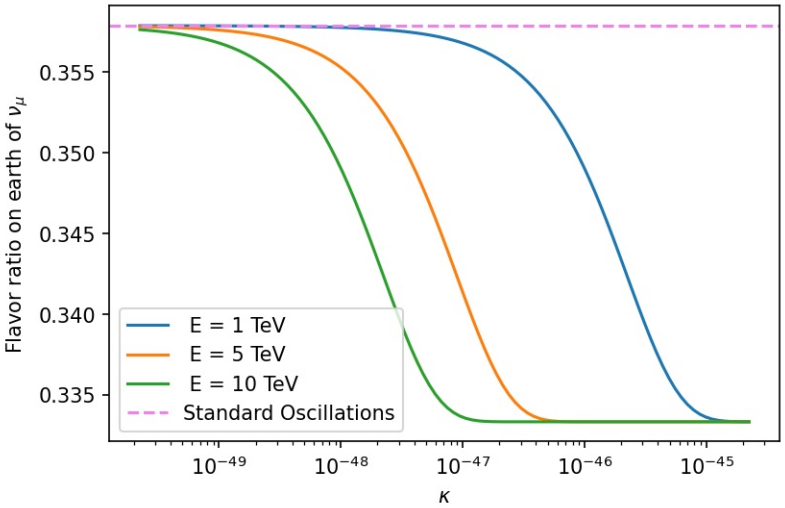

(b) Muon flavor content at Earth

Figure 3.2: The graphs of ν_e and ν_μ showcase the flavor ratios detected on earth over the energy range from [1-10] TeV in the decoherence phase space, with κ in units of GeV^{-1}. These graphs were created assuming the source ratio of 0:1:0 of high-energy neutrino emission from NGC1068 with an energy dependence of E$^{-3.2}$.

The above graphs show that neutrinos propagating in standard oscillations are not exclusively described by the decoherence parameter$(\kappa = 0)$. We can notice the effects of standard oscillations upto certain low orders of magnitude in the decoherence parameter's phase space as observed in figure (3.2a) with flavor ratios compatible with standard oscillations at $(\kappa) \leq 10^{-48}$ GeV^{-1} for neutrino energies of 1 TeV. The flavor ratios detected on earth is clearly not at unity when we consider standard oscillations. However, the ratio is strictly adhering to unity above a the decoherence $(\kappa) \geq 10^{-45}$ GeV^{-1}.

In this region, the interaction has completely put the neutrino state into full decoherence signifying complete anonymity in flavor distinction. Hence, not all magnitudes of virtual black holes will place the propagating mass eigenstates into complete decoherence. The region of interest for this research is the transition region in the decoherence space between standard oscillations and fully decohered events observed at $(\kappa) \geq 10^{-45}$ GeV^{-1}. The purpose of this thesis is thereby to set limits on the decoherence phase space to distinguish between the events detected from standard oscillations as opposed to events undergone quantum decoherence effects through interactions with a virtual black hole.

The decoherence function developed in the theoretical section behaves in an exponential manner [8-11] which can accomodate for distance(L) from the source and energy(E) of the emitted neutrinos. We can see the effect of neutrino energy towards full decoherence in figure(3.2). Higher energy neutrinos reach full decoherence at a faster rate, thereby reducing the transition window to differentiate between standard oscillations and decohered events.

$$\exp(-2\kappa t) => \exp(-2\kappa L E^n),$$

where n= -1,1,2. We will focus on the spectral index (n) = 2 for the incoming flux of neutrinos. This is a good approximation for detecting quantum decoherence effects at high energies($E_\nu \geq 1$ TeV). This can be further supported by examining the decoherence exponential function. The coherence length of these decohered neutrinos is: t(or L) $= \frac{1}{2\kappa E^n} \sim e^{-1}$ [10].

The range of the decoherence parameter's phase space could potentially range from $[0, \infty]$. Our choice for the selected range of decoherence parameter $[10^{-54} \leq \kappa \leq 10^{-40}]$ was driven by the constraints set by the source distance and the energy of the neutrinos in the transition region from standard oscillations and full decoherence. This range is ideal as we can probe $\kappa \sim 10^{-44}$ GeV^{-1} for neutrinos with energies of 1 TeV [16] defined by a E^{-2} spectrum. The transition region lies between $[10^{-47} \leq \kappa \leq 10^{-45}]$, which is where we will be focusing our attention. The ratio of the three neutrino flavors emitted by NGC1068 in consideration for this thesis were: $[\nu_e : \nu_\mu : \nu_\tau = (1:2:0); (0:1:0); (1,0,0)]$.

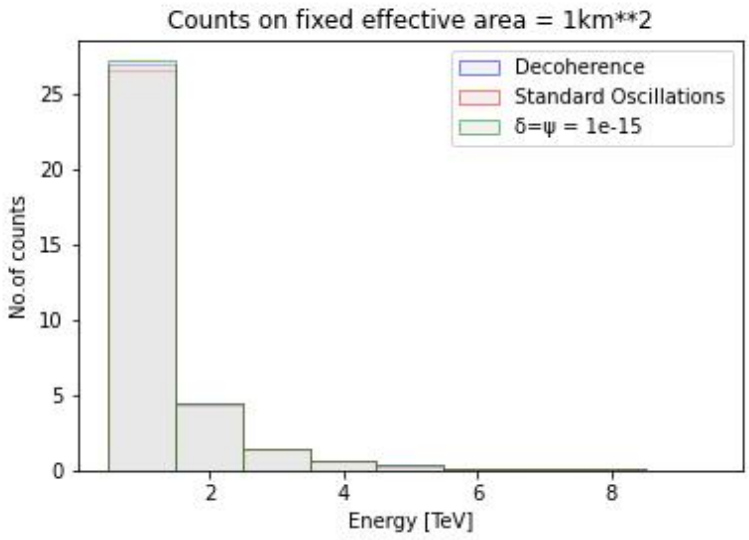

Figure 3.3: The graph shows the number of ν_μ events detected in 1 year in the energy range of 1 TeV-10 TeV following a power law spectrum of $E^{-3.2}$. The bar graphs are portraying standard oscillations, events detected from low decoherence and events seen from high decoherence ($\kappa = 10^{-45}$ GeV^{-1}). The illustration assumes a 1:2:0 source ratio of NGC1068.

Figure (3.3) is used to depict the level of difficulty in differentiating between events from standard oscillations and through quantum decoherence, even considering a highly optimistic effective area of the detector chosen for the simulations. From this graph of the detected number of ν_μ events recorded by IceCube from NGC1068, the more suitable ratios to consider for detecting quantum decoherence effects would be (1:0:0) and (0:1:0). The high count of ν_μ events at E= 1 TeV is due to the power law spectrum adapted for the energy spectrum.

3.2.1 Calculation of Event Rates In IceCube

The neutrino flux recorded by IceCube from NGC1068 is built assuming standard oscillations as shown in figure(3.4). Any deviations from the bounds of this flux will hint towards new physics or in this situations, confirm quantum decoherence effects in the three neutrino framework. The ν_μ flux calculated for the NGC0168 followed a power law spectrum [16].

$$\phi_{\nu_\mu+\bar{\nu}_\mu}(E) = \phi_o \left(\frac{E}{E_o}\right)^{-\gamma} \cdot f_{\alpha;\oplus}, \tag{3.1}$$

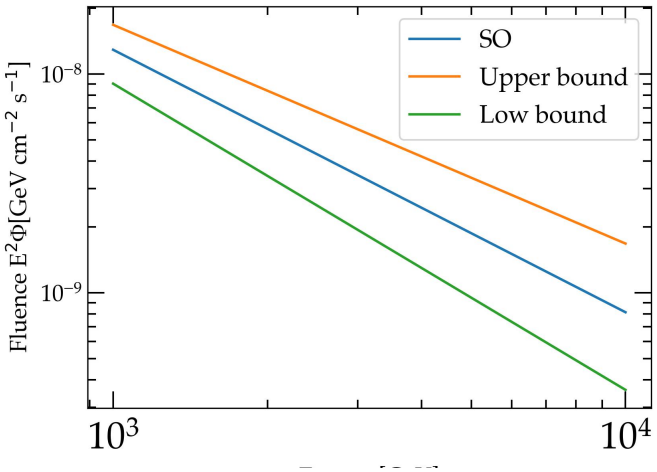

Figure 3.4: Illustration of ν_μ flux in standard oscillations (SO) from NGC1068 with the error margins included in the flux set by IceCube over the energy range of 1-10 TeV. The graph exhibits a power law of $E^{-3.2}$ [16]

here ϕ_o is the normalized flux $(5 \pm 1.5_{stat} \pm 0.6_{sys}) \times 10^{-11}$ TeV^{-1} s^{-1} cm^{-2} and $\gamma = 3.2 \pm 0.2$, is the spectral index of the flux of incoming neutrinos. The factor of $E_o = 1$ TeV is the reference energy and $f_{\alpha;\oplus}$ is the flavor ratio of the detected neutrino,

$$f_{\alpha;\oplus} = \sum_{\beta} f_{\beta,s} P_{\beta\alpha}.$$

The equation uses the average probability function developed for astrophysical neutrinos. It describes the detected flavor ratio of a neutrino(ν_α) on Earth, by taking into account the probability of the flavor ratios emitted neutrinos from the source $(f_{\beta,s})$.

The number of events calculated is an extension of equation (3.1) by integrating the incoming flux of neutrinos (ϕ(E)) over a range of energies detected in a given time period,

$$N_{\nu_\mu,i} = T \int_{E_i}^{E_i+\Delta E} dE \phi(E) A_{\text{eff}}(E) \ , \tag{3.2}$$

where T is the time(s) and A_{eff}(E) is the energy dependent effective area of IceCube. This equation is thus calculating the number of ν_μ events recorded at IceCube between two neutrino energies within a certain time period. The counts calculated for each energy in the range is separated into their respective energy bins with the size of each bin dictated by $\Delta E = 1$ TeV.

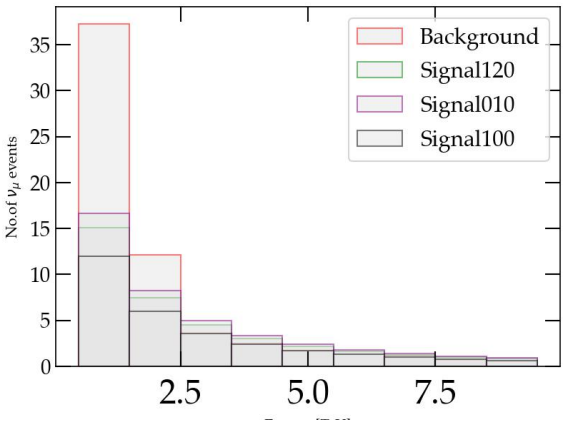

Figure 3.5: Recorded ν_μ in standard oscillations from NGC1068 for 3186 days binned into 1 TeV energy bins. The neutrinos were detected on a $E^{-3.2}$ energy spectrum. The events are calculated considering the three source ratios: (1:0:0), (0:1:0), (1:2:0) along with the background atmospheric muons.

The background atmospheric neutrino flux is used in the total flux is computed similarly.

$$N_{bg,i} = T \int_{E_i}^{E_i+\Delta E} dE \phi_{bg}(E)\ A_{eff}(E)), \tag{3.3}$$

where the ϕ_{bg}(E) is the background flux of ν_μ events recorded by IceCube. The background events were focused in the energy range of [1-10]TeV. We were recording a flux $\sim 10^{-4} GeV^{-1} cm^{-2} s^{-1} sr^{-1}$. The background events were aligned towards the declination of NGC1068 by a solid angle approximation ($\Omega \sim 1$). The NGC1068's position located in the sky is detected to be on a declination of $(0^{+0.3}_{-0.2})^\circ$ and a right ascension of $(46.7^{+0.3}_{-0.2})^\circ$ at a 95% confidence level [16].

The number of events from the background flux and NGC1068 are summed to get the total number of counts by both these fluxes in each bin. The $N_{bins} = 9$ for the energy range in consideration of [1-10] TeV. The equation for total flux detected by IceCube is the core of this thesis. We use this to calculate the number of events predicted by standard oscillations and the events from the transitional decoherence values; $[10^{-47}$ GeV$^{-1} \leq \kappa \leq 10^{-45}$ GeV$^{-1}]$. IceCube has recorded $(79^{+22}_{-20})\nu_\mu$ total events over 3186 days as shown in figure(3.5) [16]. This is the sum total of events from the signal by NGC1068 and background events from atmospheric muon neutrinos. This baseline count is used to extrapolate these events to 160 years, encapsulating the activation of future neutrino detectors under IceCube's detection time as a reference frame [23].

3.3 Statistical Analysis

The PMNS matrix governing all the functions in this thesis is constructed using the updated values of the mixing parameters.

Parameter	Mixing Angle
θ_{12}	$33.41°$
θ_{13}	$8.58°$
θ_{23}	$42.2°$
δ_{CP}	$230°$

Table 3.1: Mixing angles of the PMNS matrix set by current nu-fit prediction. [18]

The total events are separated into corresponding energy bins within a width of 1 TeV. We develop energy-dependent binned likelihood distributions of these events by assuming a true value of the decoherence(where $\kappa \geq 0$) in the decoherence parameter phase space [10^{-54} GeV$^{-1} \leq \kappa \leq 10^{-40}$ GeV^{-1}]. The likelihood function thus encapsulates the probability of an observed event given a specific set of the statistical model parameters. We adhere to this technique as likelihood functions serve as a conventional means to estimate the parameters of the statistical model based on observed events by utilizing techniques like maximum likelihood estimation [22]. For a given observed number of events in each bin (i), $N_{\text{obs},i}$, we compute the likelihood

$$L_i(\epsilon) = \frac{N_{obs,i}(\epsilon)^{N_{expt,i}} \exp(-N_{obs,i}(\epsilon))}{N_{expt,i}!}, \tag{3.4}$$

where ϵ represents the parameters on which our prediction of the expected event spectrum, $N_{\text{expt},i}$, depends.

The total likelihood accounts for the contributions across all bins, and maximizing this likelihood is equivalent to the optimization of the parameters used to determine the number of events,

$$\log L(\epsilon) = \prod_{i=1}^{N_{bins}} \log L_i(\epsilon), \tag{3.5}$$

This maximized likelihood function is thus developed through the best-fit values of the parameters represented by ϵ, explicitly given as:
(E_{min},E_{max},T,ϕ_o,n_b,γ,α,f_e,f_μ,f_τ,L,n,m,ψ, δ). These parameters thereby help build a likelihood dependent on the flux of the incoming neutrinos as well as the

detected flavor ratio on earth given by f_{ν_i}, where i corresponding to the flavor of the neutrino. Other factors taken into account was the distance (L) of the source from Earth and sorting the detected neutrino events into bins by n_b. The energy dependence (n,m) of the decoherence by the parameters ($\kappa = \psi, \delta$) was set at a fixed value of 2. The spectral index (γ) and the flux of incoming neutrinos (ϕ_o) were allowed to vary around their best-fit values for an optimal likelihood distribution.

We use the maximized likelihood distribution in the least squares method(LS) for the final analysis [20,22]. These optimized likelihoods are observed to be following a Gaussian distribution around the true value of the decoherence parameter. The maximum likelihood and the least squares method are proportional to each other as outlined in equation(3.6). Thus, minimizing the χ^2 distribution will be equivalent to maximizing the likelihood for a particular(true) value of the decoherence parameter.

$$\chi^2(\epsilon) = -2 \log L(\epsilon) \tag{3.6}$$

We accommodate for the uncertainty associated with the two parameters of ϵ, namely the normalization factor of the flux and the energy spectral index of the incoming flux. The rest of the parameters are assumed to be at their best-fit value.

$$\chi^2_F = -2 \log L(\epsilon) + \left(\frac{\phi_c - \phi_o}{\delta\phi_o}\right)^2 + \left(\frac{\gamma_c - \gamma_o}{\delta\gamma}\right)^2 \tag{3.7}$$

Here ϕ_o and γ_o are the best-fit values of the normalization and energy spectral index respectively with their associated uncertainties denoted in the denominator. $\phi_o = (5 \pm 1.5_{stat} \pm 0.6_{sys}) \times 10^{-11}\ TeV^{-1}s^{-1}cm^{-2}$ and $\gamma = 3.2 \pm 0.2$ [16]. These terms added to the χ^2 distribution act as 'pull terms' to skew the likelihood functions towards the best-fit value of these parameters.
These modified χ^2_F distributions were created by minimizing the χ^2 distribution for a true value of decoherence by utilizing the optimal values of the two parameters (ϕ, γ = P) calculated around their best-fit values. These minimized χ^2 distributions around the optimal values ('P') were interpolated into a single χ^2 distribution which was further minimized over the decoherence phase space to create the final χ^2_F distribution centered around the true decoherence value. The minimizer used in these calculations was a scipy script for optimization of a 1D array. The confidence limits($\Delta\chi^2$) set on the decoherence values in

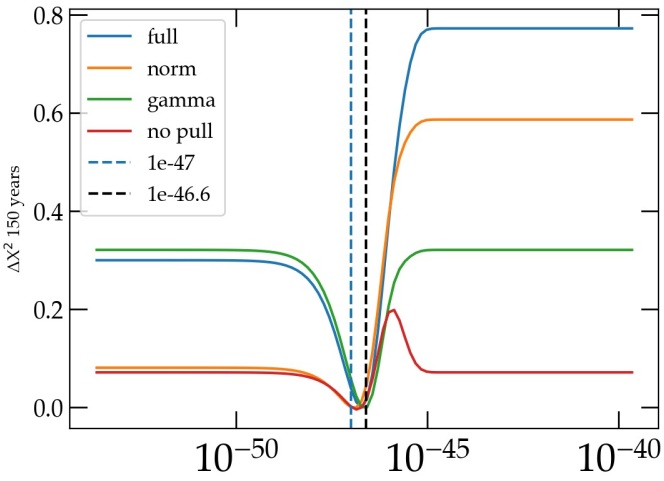

Figure 3.6: The limit set on a true decoherence parameter of 10^{-47} GeV^{-1} over an exposure period of 150 years of ν_μ events. We are considering the source ratio of 0:1:0 in this situation. The graph depicts the influence of each P parameter on the level of the confidence limit we can set on $\chi^2_F(\epsilon)$ distribution where we assume the presence of just one variable from P to be active. The 'full' suggests both the variables are active while no pull terms is suggesting the absence of both the variables of P.

the transition region$(10^{-47} \leq \kappa \leq 10^{-46})$ were set on these new optimized χ^2_F distributions. These distributions will give us realistic limitations on the possibility of detecting quantum decoherence through the number of events detected by IceCube. Evaluating these χ^2 distributions at their minimum values will help set limits on the true value of the decoherence [20]. The confidence limit on the true value of decoherence is quantified by $\Delta\chi^2$ [20-22],

$$\Delta\chi^2 = \chi^2_F - \chi^2_{min}, \tag{3.8}$$

where we try to set limits upto 3σ on the χ^2_{min} distributions with respect to the decoherence parameter (κ). A higher deviation contributes to a better confidence level on the best fit value of the decoherence parameter.

Confidence Limit	Value of $\Delta\chi^2$
68%	1
95%	4
99.7%	9

Table 3.2: The level of confidence we can place based on the value of $\Delta\chi^2$. The confidence limits for a $\Delta\chi^2$ distribution is determined on a single parameter (κ) in consideration when minimizing the χ^2 distribution. [21]

We can see the optimized $\chi^2_F(\epsilon)$ for the best fit values of the pull terms: ϕ_o and γ, given by the 'full' curve and the 'no pull' curve portrays the limit on the flux without the pull factors in figure(3.6). We can notice the importance of the pull terms from the graph and the improvement on the limit set on the true value of decoherence considered in this situation with the inclusion of the optimized values. Thus in this situation, optimizing the χ^2 distributions on the pull terms has quadrupled our chance of setting a limit on the decoherence value. The figure with just the normalization factor active seems to be the biggest contributor to the pull factor towards the optimized neutrino flux given by the 'full' graph. However, when we just have the gamma active, it shows equal possibility of neutrino events detected from decohered interactions at 10^{-47} GeV^{-1}. The influence of the two optimized parameters on the flux can be further seen in the limits set considering a true decoherence of 10^{-46} GeV^{-1} and 10^{-47} GeV^{-1} for a source ratio of 1:0:0 in the results section.

3.3.1 Absence of Atmospheric background flux

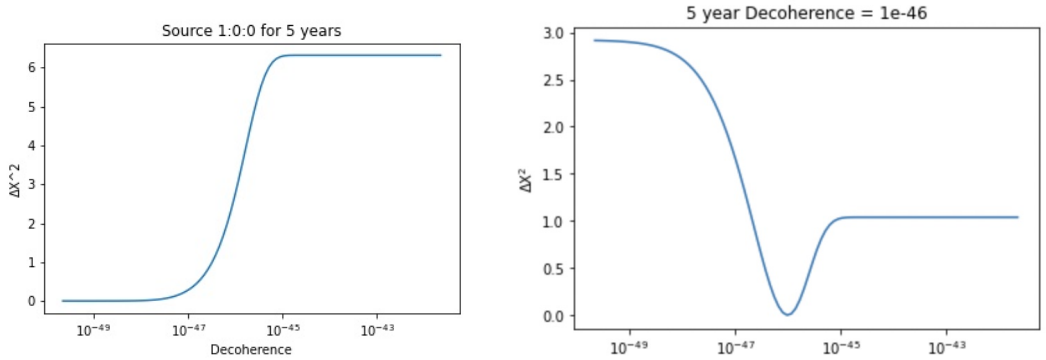

(a) Standard oscillations

(b) Assume True value of $\kappa = 10^{-46}$ GeV^{-1}

Figure 3.7: These $\Delta\chi^2$ distributions were developed assuming the source ratio of NGC1068 to be 1:0:0 over an exposure time of 5 years by considering the current event rate of ν_μ by the source to stay constant.The above graphs represent the limits we can set on the true value of decoherence by evaluating $\delta\chi^2$ distributions considering the true decoherence of $\kappa = 0$ and $\kappa = 10^{-46}$ GeV^{-1} respectively.

These illustrations are considering ideal situations i.e. with no background flux of atmospheric muons, of standard oscillations and decohered events detected on earth. We expect to see neutrinos propagating in low decoherence values to behave in the same manner as standard oscillations as seen in figure (3.2). However, neutrinos interacting with VBH of a magnitude $\geq 10^{-48}$ GeV^{-1} incorporates observable decoherence effects, which is evident in figure (3.6a)

displaying subtle deviations from standard oscillations. We can set confidence limits on the true value of decoherence in both situations. We are able to set upper limits in the decoherence phase space up to 2σ for events detected by standard oscillations emitted from NGC1068. We are also able to set a lower bound on the true value of decoherence up to 1σ over this particular run-time of IceCube with hints of measuring/bounding this value over higher exposure times. The $\Delta\chi^2$ graph for standard oscillations clearly portrays the transition region between these two processes of standard oscillations and decoherence events, with signs of full decoherence at 10^{-45} GeV^{-1}.

In perfect conditions when the background atmospheric neutrinos are negligible and the normalized incoming flux and the spectral index of the emitted neutrinos are the best fit values calculated by IceCube [16], we can set 3σ confidence limits in the decoherence space on standard oscillations and bound the decoherence parameter of the transition region.

Figure 3.7 shows that if the true value of kappa is 10^{-47} GeV^{-1}, we would only be able to set upper limits on its value. When we consider the true value of κ $=10^{-46}$ GeV^{-1} , we can bound the value, proving measurement possibility of this particular decoherence by the events detected on earth. These limits are however idealistic and will be altered with the introduction of the background atmospheric muon flux and by varying the chi square distributions around the pull terms for a realistic bound on the decoherence value over time.

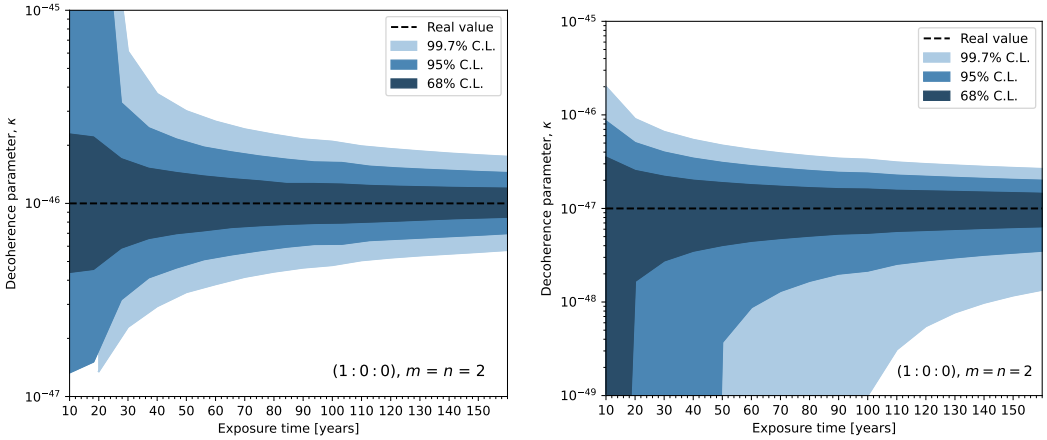

(a) Bounds with true decoherence = 10^{-46} GeV^{-1}

(b) Bounds with true decoherence = 10^{-47} GeV^{-1}

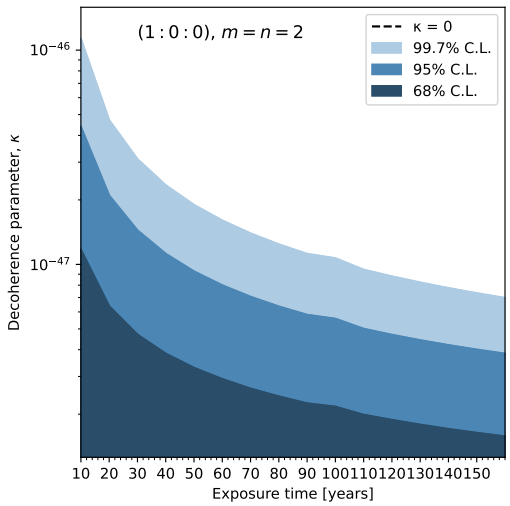

(c) Upper limits on Standard Oscillations

Figure 3.8: The above graph shows the limits set on a decoherence value = 10^{-46} GeV^{-1} , 10^{-47} GeV^{-1} and standard oscillations respectively if we consider the source ratio of NGC1068 = (1:0:0) over an exposure time of 160 years encapsulating all the possible start period of future neutrino detectors. These results are created assuming ideal situations.

4 Results

The analysis of determining quantum decoherence effects in high-energy neutrinos emitted from NGC1068 has led us to conclude the optimal source ratio for establishing a limit on the decoherence value in the transition zone as 1:0:0.

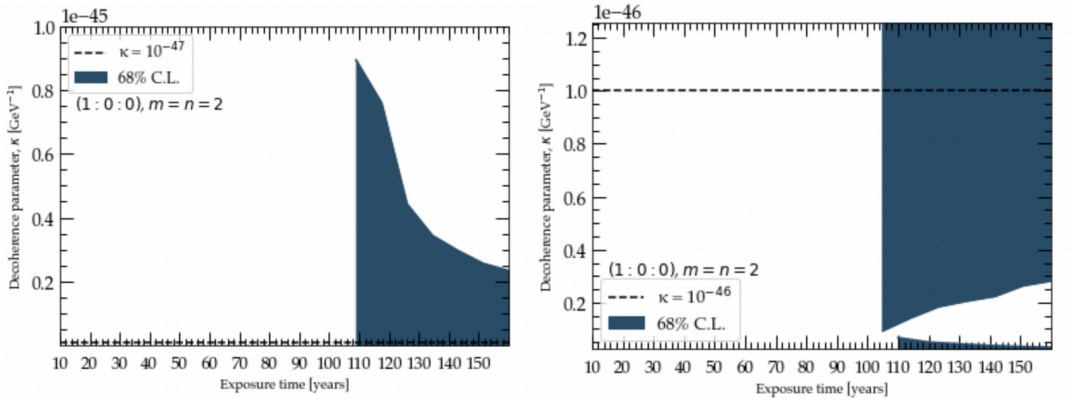

(a) Bounds on $\kappa = 10^{-47}$ GeV^{-1}

(b) Bounds on $\kappa = 10^{-46}$ GeV^{-1}

(c) Bounds on exclusion of standard oscillations

Figure 4.1: The above graph shows the limits set on a decoherence value $= 10^{-47}$ GeV^{-1} , 10^{-46} GeV^{-1} and standard oscillations respectively if we consider the source ratio of NGC1068 = (1:0:0) over an exposure time of 160 years encapsulating all the possible start period of future neutrino detectors. The bounds were determined assuming a behavior of E$^{-3.2}$ of energy dependence of the incoming flux of neutrinos for the interaction.

We are able to set 1σ limits in the decoherence phase space for all three sce-

narios portrayed in figure (4.1). The graphs illustrates a gap in time preceding its first observation in all three scenarios. This would directly revert back to the confidence limits we needed to satisfy as prescribed by $\Delta\chi^2$ to claim a measurement. Unfortunately, the disparity between the χ^2 distributions, compared to their minimum values for these decoherence parameters, consistently remained below one within the vacant regions on the graphs.

Standard oscillations could be excluded in the region of 10^{-46} GeV^{-1} with the lower bound stretching up to $10^{-47.314}$ GeV^{-1}. This led us to set a lower bound when we considered the true decoherence of 10^{-46} GeV^{-1} with the best limit to be of $10^{-46.55}$ GeV^{-1}. However the lower bound of $10^{-47.17}$ GeV^{-1} observed in figure (4.1b) is highly peculiar even though established with a reduced chance of detection as per the $\Delta\chi^2$ distribution. These limits would suggest the detection of neutrino events decohered at a magnitude of 10^{-46} GeV^{-1} to have the same signature as if it interacted with a virtual black hole with a magnitude of 10^{-50} GeV^{-1}. This limit however may be excluded with a higher number of ν_μ counts detected at IceCube by the NGC1068. We also could set an upper limit on the true value of decoherence of 10^{-47} GeV^{-1} with its best bound at $10^{-45.63}$ GeV^{-1}. This value of decoherence was particularly difficult to bound since standard oscillations had already excluded a major portion of the decoherence space between [10^{-47} GeV^{-1} - $10^{-47.9}$ GeV^{-1}]. Approximately 70$\%$ of the phase space within this region was excluded by standard oscillations, leaving only 30$\%$ available for assessment.

The transition zone for differentiating between standard oscillations and decohered events was altered to a new range from [10^{47} GeV$^{-1} \leq \kappa \leq 10^{-45}$ GeV^{-1}] $\rightarrow$ [$10^{-47.3}$ GeV$^{-1} \leq \kappa \leq 10^{-46.3}$ GeV^{-1}] at a confidence limit of 1σ. These limits are bound to improve over time with the observation of more high-energy neutrinos emanating from NGC1068 and thereby excluding a bigger portion within decoherence space from standard oscillations. Although the limits set on 10^{-47} GeV^{-1} are quite close to the full decoherence value of 10^{-45} GeV^{-1} , the limits are improving at a faster rate than the limits set on 10^{-46} GeV^{-1}. The lower bound set on 10^{-46} GeV^{-1} is roughly improving linearly over time hinting towards an upper bound, thereby finally be able to measure the value. Currently, this scenario has the highest potential in detecting quantum decoherence in neutrinos.

The other two source ratios (0:1:0, 1:2:0) considered are well under any confidence regions and would need more time to set any limits as seen in figure(4.2) with the values of $\Delta\chi^2$ well under 1σ. The graphs clearly favor the source ratio of 0:1:0 after 1:0:0, even though we would need a higher

data sample of ν_μ neutrinos to be able to claim a 68% confidence limit and a possible measurement capability. The decoherence value of 10^{-46} GeV^{-1} shows a better chance of being bound as opposed to 10^{-47} GeV^{-1}. Unfortunately, the pion decay source (1:2:0) has a very low chance of detecting quantum decoherence. The magnitude of $\Delta\chi^2$ values for both values of decoherence are relatively same with a slightly better chance of detection at higher values of decoherence. Even if the magnitude could be amplified to set any confidence limits, the current graph topography suggests no measurement capability by the least squares method of the decoherence value but just the exclusion of an area in the decoherence phase space where events from this decoherence wouldn't be created by the ν-VBH interaction.

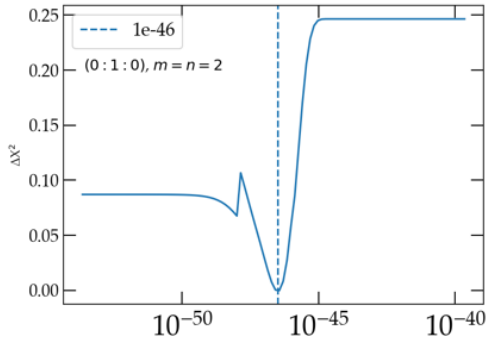

(a) Bounds for 0:1:0 source ratio

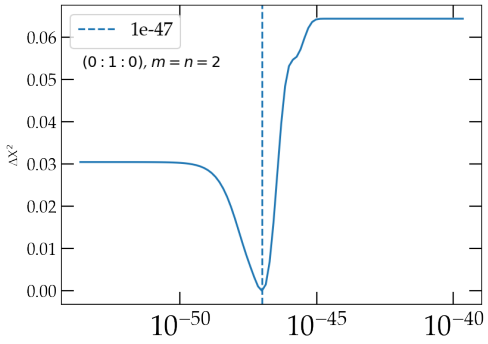

(b) Bounds for 0:1:0 source ratio

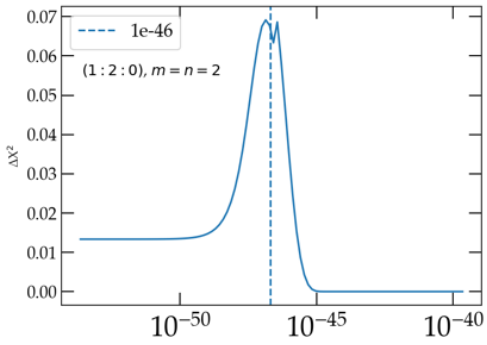

(c) Bounds for 1:2:0 source ratio

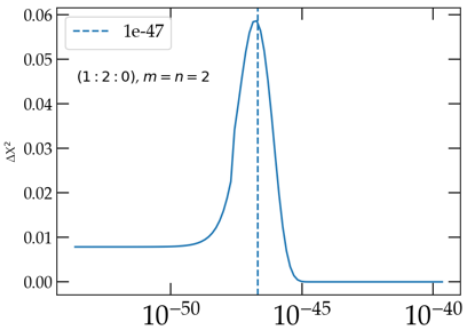

(d) Bounds for 1:2:0 source ratio

Figure 4.2: The above graph shows the $\Delta\chi^2$ distributions of decoherence values of 10^{-47} GeV^{-1} and 10^{-46} GeV^{-1} for a period of 160 years for the two source ratios: 0:1:0 and 1:2:0. The energy dependence of incoming flux of neutrinos followed a E$^{-3.2}$ behavior.

There is merit in determining the effects of quantum decoherence through the number of events detected at a neutrino detector. We could only use this technique due to the point source nature of NGC1068 which helped us eliminate several uncertainties associated with astrophysical neutrino fluxes.

Even though the constraints set on the decoherence values may not been significant, it certainly pushed us towards the right direction. This experiment gave us definitive confirmation on the chances of distinguishing quantum gravity effects by IceCube in propagating mass eigenstates of astrophysical muon neutrinos. The limits may differ if we had assumed an equally probable mass state selection after the ν-VBH interaction.

5 Summary and Outlook

The limits calculated for the source ratios were set under the assumption that IceCube would be the exclusive detector used for high-energy neutrino detection. However, with the emergence of new and improved neutrino detectors planned to launch in the near future, the time period taken to set these bounds would significantly be reduced [23]. One of these detectors is the next version of IceCube named IceCube Gen-2 planned to be active by 2032 [11]. This detector volume of 8 km^3 is 8 times bigger than the current IceCube, thereby improving the rate of neutrino detections by an whole order of magnitude [11]. Just like the Gen-2 proposal, there is another detector of similar volume called TRIDENT [12,13] being launched around the same time in China, with promises of locating the NGC1068 within its first year of operation. Additionally, upcoming detectors namely Baikal-GVD, KM3NeT, and P-ONE, also larger than IceCube, will contribute towards this objective. Multiple neutrino telescopes are even uniting their efforts, witnessed in the Global Neutrino Network(GNN) comprised of four partners: The ANTARES, Baikal-GvD, IceCube and KM3NeT [14].

The stochastic nature of decoherence in astrophysical high-energy neutrinos forces the loss of coherence between the density states describing the multitude possibilities of quantum states of a propagating neutrino [8,9,10]. This loss thereby left sensitivity to only two out of the eleven decoherence parameters we could assess through the number of events detected at IceCube[8,9] as seen in chapters (2.3-3). Despite the advancements in neutrino detector technology, it is possible that we may not achieve sensitivity to the other decoherence parameters if we consider astrophysical neutrinos. Atmospheric neutrinos, with comparable energies but shorter baselines, may provide access to those decoherence parameters.[15].

The ν_μ events detected by IceCube from NGC1068 [16] come together with a heavy background noise of atmospheric muon events. The background flux managed to reduce the confidence limits by a factor of 2σ as seen from figures (3.8,4.1). With our current technology, it is strongly recommended to

investigate the quantum decoherence effects in high-energy neutrinos emitted by NGC1068 through ν_e events as well, thereby increasing the size of the data sample. Studying the tracks along with the cascades left by ν_e events should be the next step in this experiment. While cascades come with their own disadvantages like poor angular resolution, they do exhibit a low background noise [17].

The low level of background noise will heed to improved limits as our current data sample was driven by the background noise in the energy range of 1 TeV - 3 TeV. The angular resolution of these cascades could be improved if we target the cascades made on the path of the muon tracks. Detecting tracks and showers would allow to search for decoherence not only through changes in the energy spectrum, but also to the flavor content of the flux. Signs of quantum decoherence effects in cascades can be measured in altered energy spectrum, momentum or even angular distribution of the secondary particles from standard expectations.

Detection of quantum gravity effects in neutrinos is a formidable proposition demanding advanced techniques and most probably, a collective collaboration. To maximize efficiency, incorporating the inclusion of other neutrino telescopes is essential for comprehensive insights, especially if we plan to work exclusively with ν_μ events. With the current efficiency of our neutrino detectors along with the anticipated activation of detectors in the near future, the pursuit of unveiling quantum gravity effects through quantum decoherence in neutrino systems would be a collective journey as opposed to an individual experiment; thereby pushing the boundaries in the realm of astroparticle physics.

Appendix A

6

6.0.1 Physical Constants

In this thesis, we assume natural units:

$$c = \hbar = 1,$$

where 'c' represents the speed of light and $\hbar$ is planck's constant. The physical constants used in this thesis were extracted from the Review of Particle Physics listed in the table below with the 1σ uncertainty of the last digits provided in the parenthesis.

Description	Value
Reduced Planck Constant ($\hbar$)	6.58211915(56) $\times$ 10^{-16} eV s
Speed of Light (c)	299792458 ms^{-1}
Conversion Constant ($\hbar$c)	1.97326968(17) $\times$ 10^{-5} eV cm
Planck Mass	1.22090(9)$\times 10^{19}$ GeV
Planck Length	1.616255(18) $\times$ 10^{-35} m
Planck Time	5.391247(60)$\times$ 10^{-44} s
Parsec (pc)	3.0856775807 $\times$ 10^{16} m
Muon mass	105.658369(9) MeV
Muon Lifetime	2.19703(4)$\times$ 10^{-6} s
Tau mass	1776.99 MeV
Electron mass	0.510998918 (44) MeV

Table 6.1: Physical constants.[1,2,3,4]

The conversion factors used for natural units were guided by [5].

6.0.2 Density Matrix Formalism

The generators (λ_i) in the SU(3) basis for the formalism of the density matrix (equation(2.22)) were the Gell-Mann matrices [6] along with the identity

matrix to accommodate for standard oscillations. The density state (ρ_0) describing standard oscillations was equal to $\frac{2}{3}$ by imposing the Tr[ρ] = 1. The trace is preserved during evolution and thus ρ_0 is a constant. The remaining eight terms of the density matrix was solved by equation(2.22) influenced by the initial pure state [7,8] of a flavor neutrino given:

$$\rho_{\nu_\alpha}(0) = \begin{bmatrix} U_{\alpha1}^2 & U_{\alpha1}U_{\alpha2} & U_{\alpha1}U_{\alpha3} \\ U_{\alpha2}U_{\alpha1} & U_{\alpha2}^2 & U_{\alpha2}U_{\alpha3} \\ U_{\alpha3}U_{\alpha1} & U_{\alpha3}U_{\alpha2} & U_{\alpha3}^2 \end{bmatrix}, \tag{6.1}$$

and writing the evolution of the 3x3 density matrix[8] explicitly as such:

$$\rho(t) = \frac{1}{2}\begin{bmatrix} \rho_0 + \rho_3 + \frac{\rho_8}{\sqrt{3}} & \rho_1 - \Im\rho_2 & \rho_4 - \Im\rho_5 \\ \rho_1 + \Im\rho_2 & \rho_0 - \rho_3 + \frac{\rho_8}{\sqrt{3}} & \rho_6 - \Im\rho_7 \\ \rho_4 + \Im\rho_5 & \rho_6 + \Im\rho_7 & \rho_0 - \frac{2\rho_8}{\sqrt{3}} \end{bmatrix} \tag{6.2}$$

The diagonal terms refer to as the population while the off-diagonal terms represent the coherence of the matrix which will contain the phase information [8,9]. The long distance behavior of astrophysical neutrinos was visible in this matrix as all coherence was lost amongst other density states. The loss of coherence is justified by noticing the non-zero decoherence parameters in the off-diagonal terms damping the oscillations to zero but also preserving the diagonal terms of the density matrix. The non-zero decoherence terms of the diagonal produces a damping of the non-oscillatory terms in a $\frac{1}{X}$ manner, where X is the number of neutrino families as observed in the figure(3.2) over a long distance[9]. This allowed us sensitivity to just two states containing information on the degree of decoherence deviated from standard oscillations (ρ_0) [8,9]. The evolution of the density matrix components can be noticed clearly when we redefine the 8x8 decoherence parameter matrix as an exponential function mirroring the damping behavior of the decoherence parameter on neutrino oscillations and state selection process. The effect of decoherence on each component of the density can be written as: M = $\exp(-2Lt)$ [8], where L is the 8x8 matrix. The exponentiated M matrix will heed the solutions to the time evolved density components ($\dot{\rho_1} \rightarrow \dot{\rho_8}$).

$$\rho_i(t) = \rho_i(0)M_{i1}+\rho_i(0)M_{i2}+\rho_i(0)M_{i3}+\rho_i(0)M_{i4}+\rho_i(0)M_{i5}+\rho_i(0)M_{i6}+\rho_i(0)M_{i7}+\rho_i(0)M_{i8},$$

where $\rho_i(0)$ represents the component of the initial density matrix given by equations(6.1-6.2).

6.0.3 Dependent Parameters of Functions

The transitional probability $(\nu_\alpha \rightarrow \nu_\beta)$ used was dependent on these parameters for detecting quantum decoherence effects in the events recorded at IceCube [8].

$$P_{\alpha\beta}(\alpha, \beta, L, E, n, m, \psi, \delta) \tag{6.3}$$

Utilizing the source information of NGC1068. Distance(L) of NGC1068 from earth($2.23 \times 10^{39} GeV^{-1}$) and energy range of the neutrinos in consideration (1 TeV $\leq E_\nu \leq$ 10 TeV) [16],

This probability was utilized for determining the flavor ratio composition (α) on earth [7],

$$F_{\alpha,\oplus}(\alpha, f_e, f_\mu, f_\tau, E, L, n, m, \psi, \delta) \tag{6.4}$$

The flux of the emitted neutrinos by NGC1068 was generated by using a generic power law spectrum using the flavor ratio composition [16]. The flux has an additional dependence on the normalization factor of the incoming neutrinos and spectral index of the emitted neutrinos.

$$\phi(E)(\phi_o, \gamma, \alpha, f_e, f_{mu}, f_\tau, E, L, n, m, \psi, \delta) \tag{6.5}$$

The number of muon neutrinos was thus extracted by using the trapezoidal rule of integration over energy on the incoming ν_μ flux.

$$N_{\nu_\mu}(E_{min}, E_{max}, T, \phi_o, \gamma, \alpha, f_e, f_\mu, f_\tau, L, n, m, \psi, \delta) \tag{6.6}$$

However the dependent parameters used to calculate the number of atmospheric neutrino events was just energy of the neutrinos and time period.

$$N_{bg}(E_{min}, E_{max}, T) \tag{6.7}$$

7 Bibliography

1) S. Eidelman et al. (Particle Data Group), Phys. Lett. B592, 1 (2004)

2) "2018 CODATA Value: Planck length". The NIST Reference on Constants, Units, and Uncertainty. NIST. 20 May 2019. Retrieved 20 May 2019.

3)"2018 CODATA Value: Planck mass". The NIST Reference on Constants, Units, and Uncertainty. NIST. 20 May 2019. Retrieved 20 May 2019.

4) "2018 CODATA Value: Planck time". The NIST Reference on Constants, Units, and Uncertainty. NIST. 20 May 2019. Retrieved 20 May 2019.

5) A. D. Dolgov, "Neutrinos in Cosmology," Phys. Rept. 370 (2002) 333-535 [arXiv:hep-ph/0202122, doi:10.1016/S0370-1573(02)00139-4].

6) Sanchez, Jesus. (2023). Gell-Mann Matrices (Strong Force Interaction) in Geometric Algebra Cl(3,0). 10.13140/RG.2.2.17573.27365.

7) Giunti, Carlo, and Chung W. Kim, Fundamentals of Neutrino Physics and Astrophysics (Oxford, 2007; online edn, Oxford Academic, 1 Jan. 2010), https://doi.org/10.1093/acprof:oso/9780198508717.001.0001, accessed 24 Nov. 2023

8)P. Mehta and W. Winter, "Interplay of energy-dependent astrophysical neutrino flavor ratios and new physics effects," J. Cosmol. Astropart. Phys. 03 (2011) 041 [arXiv:1101.2673, doi:10.1088/1475-7516/2011/03/041].

9) T. Stuttard and M. Jensen, "Neutrino decoherence from quantum gravitational stochastic perturbations," Phys. Rev. D 102, 115003 (2020), [doi:10.1103/PhysRevD.102.115003].

10) T. Stuttard, "Neutrino signals of lightcone fluctuations resulting from fluctuating spacetime," Phys. Rev. D 104, 056007 (2021) [doi:10.1103/PhysRevD.104.056007].

11) IceCube-Gen2 Collaboration, "IceCube-Gen2 Project," https://www.icecube-gen2.de/project/index$_eng$.html (Accessed [15-11-2023]).

12) Shanghai Jiao Tong University, "Trident: A Generative Model for Artificially Creating Training Data," https://trident.sjtu.edu.cn/en (Accessed [15-11-2023]).

13) Z. P. Ye et al, A multi-cubic-kilometre neutrino telescope in the western Pacific Ocean, Nature Astronomy (2023). DOI: 10.1038/s41550-023-02087-6

14) Global Neutrino Network, "Home," https://www.globalneutrinonetwork.org/ (Accessed [15-11-2023]).

15) IceCube Collaboration, et al., "Searching for Decoherence from Quantum Gravity at the IceCube South Pole Neutrino Observatory," arXiv:2308.00105 [hep-ex] (2023).

16) IceCube Collaboration, et al., "Evidence for neutrino emission from the nearby active galaxy NGC 1068," Science, vol. 378, no. 6619, pp. 538–543, Nov 2022, doi: 10.1126/science.abg3395.

17) IceCube Collaboration, Halzen, F, and Klein, S. IceCube: An Instrument for Neutrino Astronomy. United States: N. p., 2010. Web.

18) Ivan Esteban, M.C. Gonzalez-Garcia, Michele Maltoni, Thomas Schwetz, Albert Zhou, "The fate of hints: updated global analysis of three-flavor neutrino oscillations," Journal of High Energy Physics, vol. 2020, no. 9, p. 178, Sep 2020, doi: 10.1007/JHEP09(2020)178.

19) Press, Astronomy 45 Course Notes Introduction to Astrophysics. (1997). Title of the Webpage. Retrieved from https://www.lanl.gov/DLDSTP/ay45/ay45top.html

20) Particle Data Group. (2020). Review of Particle Physics 2020 - Statistics. Retrieved from https://pdg.lbl.gov/2020/reviews/rpp2020-rev-statistics.pdf

21) NASA/IPAC Extragalactic Database (NED). (1996). The Large Scale Structure of the Universe (Contents). Published in Q. Jl R. astr. Soc., 37, 519-563. Retrieved from https://ned.ipac.caltech.edu/level5/Wall2/Walcontents.html

22) DeTar, C. (n.d.). Curve Fitting - Least Squares Method. Retrieved from https://web.physics.utah.edu/ detar/phys6720/handouts/curvefit/curvefit/node2.html

23) Fiorillo, D. F. G., Bustamante, M. (2023). Bump hunting in the diffuse flux of high-energy cosmic neutrinos. Physical Review D, 107(8), 083008. https://doi.org/10.1103/PhysRevD.107.083008

24)M. G. Aartsen et al., Observation of High-Energy Astrophysical Neutrinos in Three Years of IceCube Data, Phys. Rev. Lett. 113 (2014) 101101 [arXiv:1405.5303

25) Hill, G. C. (2015). "First detection of high-energy astrophysical neutrinos with IceCube." In XXVI International Conference on Neutrino Physics and AstroPhysics: Neutrino 2014 (AIP Conference Proceedings, Vol. 1666, No. 1, p. 040001). American Institute of Physics. doi: 10.1063/1.4915550. ADS Link.

26) dos Santos, M. V., de Holanda, P. C., Dedin Neto, P., Kemp, E. (2023). "On the Effects of Quantum Decoherence in a Future Supernova Neutrino Detection." arXiv preprint arXiv:2306.17591.

27) Ackermann, M., Ahlers, M., Anchordoqui, L., Bustamante, M., Connolly, A., Deaconu, C., ... Wissel, S. (2019). "Astrophysics Uniquely Enabled by Observations of High-Energy Cosmic Neutrinos." arXiv preprint arXiv:1903.04334.

28) Davis, R., Harmer, D. S., Hoffman, K. C. (1968). "Search for Neutrinos from the Sun." Phys. Rev. Lett., 20(21), 1205–1209. DOI: 10.1103/PhysRevLett.20.1205

29) Aartsen, M. G. et al. (IceCube Collaboration). "Evidence for High-Energy Extraterrestrial Neutrinos at the IceCube Detector." Science, vol. 342, no. 6161, 2013, pp. 1242856. DOI: 10.1126/science.1242856.

30) A. Burrows and J. M. Lattimer, "Neutrinos from SN 1987A," Astrophysical Journal Letters, vol. 318, Jul. 1987, p. L63. DOI: 10.1086/184938.

31) M. Aartsen et al. (IceCube Collaboration), "Neutrino emission from the direction of the blazar TXS 0506+056 prior to the IceCube-170922A alert," Science, vol. 361, no. 6398, Jul. 2018, pp. 147–151. DOI: 10.1126/science.aat2890.

32) Y. Fukuda et al., Evidence for oscillation of atmospheric neutrinos, Phys. Rev. Lett. 81 (1998) 1562 [hep-ex/9807003].

33) Ellis R Owen, Idunn B Jacobsen, Kinwah Wu, Pooja Surajbali, Interactions between ultra-high-energy particles and protogalactic environments, Monthly Notices of the Royal Astronomical Society, Volume 481, Issue 1, November 2018, Pages 666–687, https://doi.org/10.1093/mnras/sty2279

34) Neutrinos from active galactic nuclei as a diagnostic tool C. Schuster, M. Pohl and R. Schlickeiser AA, 382 3 (2002) 829-837 DOI: https://doi.org/10.1051/0004-6361:20011670

35) S. Hu mmer, M. Ru ger, F. Spanier, and W. Winter. Simplified models for photohadronic interactions in cosmic accelerators. Astrophys.J., 721:630–652, 2010.

36) R. C. Hickox and D. M. Alexander, "Obscured Active Galactic Nuclei," Ann. Rev. Astron. Astrophys., vol. 56, pp. 625–671, 2018, DOI: 10.1146/annurev-astro-081817-051803.

37) M.G. Aartsen et al. (IceCube Collaboration), "Time-Integrated Neutrino Source Searches with 10 Years of IceCube Data," Phys. Rev. Lett. 124, 051103 (2020), DOI: 10.1103/PhysRevLett.124.051103.

38) Guépin, Claire, Kumiko Kotera, and Foteini Oikonomou. "High-energy Neutrino Transients and the Future of Multi-messenger Astronomy." arXiv preprint arXiv:2207.12205 (2022).

39) Inoue, Susumu, Matteo Cerruti, Kohta Murase, and Ruo-Yu Liu. "High-energy Neutrinos and Gamma Rays from Winds and Tori in Active Galactic Nuclei." arXiv preprint arXiv:2207.02097 (2022).

40) SEDS. "Messier 77 - Spiral Galaxy." Students for the Exploration and Development of Space (SEDS), http://www.messier.seds.org/m/m077.html

41) Acero, M. A., Adamson, P., Aliaga, L., Alion, T., Allakhverdian, V., Altakarli, S., ... Zwaska, R. (2019). First measurement of neutrino oscillation parameters using neutrinos and antineutrinos by NOvA. Physical Review Letters, 123(15), 151803. http://dx.doi.org/10.1103/PhysRevLett.123.151803

42) The T2K Collaboration. Constraint on the matter–antimatter symmetry-violating phase in neutrino oscillations. Nature 580, 339–344 (2020). https://doi.org/10.1038
020-2177-0

43) A. Loureiro et al., "Upper Bound of Neutrino Masses from Combined Cosmological Observations and Particle Physics Experiments," Phys. Rev. Lett. 123, 081301 (2019), [http://dx.doi.org/10.1103/PhysRevLett.123.081301]

44) T. Ohlsson, Equivalence between gaussian averaged neu- trino oscillations and neutrino decoherence, Physics Let- ters B 502, 159 (2001).